

Accepted Manuscript

Identification of 3-(benzazol-2-yl)quinoxaline derivatives as potent anticancer compounds: Privileged structure-based design, synthesis, and bioactive evaluation *in vitro* and *in vivo*

Qing-Qing Liu, Ke Lu, Hai-Miao Zhu, Shi-Lin Kong, Jing-Mei Yuan, Guo-Hai Zhang, Nan-Ying Chen, Chen-Xi Gu, Cheng-Xue Pan, Dong-Liang Mo, Gui-Fa Su

PII: S0223-5234(19)30004-2

DOI: <https://doi.org/10.1016/j.ejmech.2019.01.004>

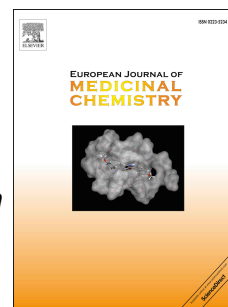
Reference: EJMECH 11011

To appear in: *European Journal of Medicinal Chemistry*

Received Date: 25 October 2018

Revised Date: 27 December 2018

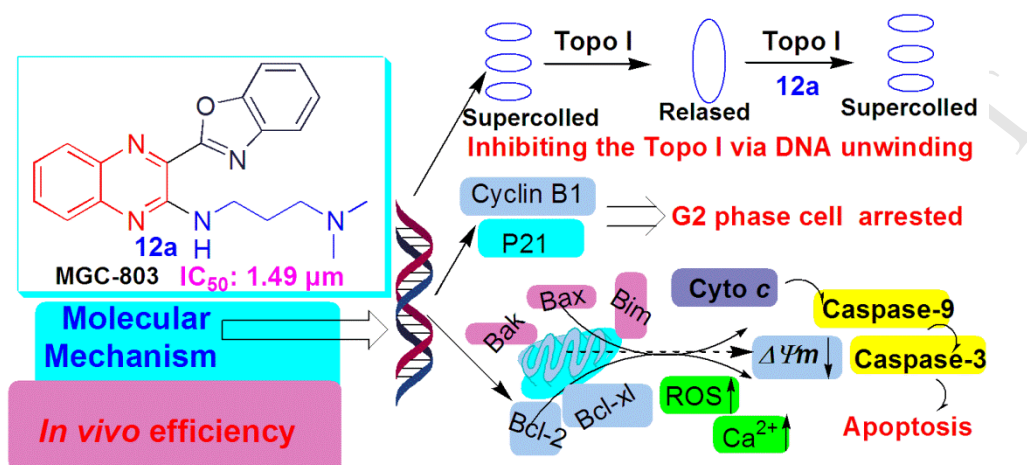
Accepted Date: 2 January 2019



Please cite this article as: Q.-Q. Liu, K. Lu, H.-M. Zhu, S.-L. Kong, J.-M. Yuan, G.-H. Zhang, N.-Y. Chen, C.-X. Gu, C.-X. Pan, D.-L. Mo, G.-F. Su, Identification of 3-(benzazol-2-yl)quinoxaline derivatives as potent anticancer compounds: Privileged structure-based design, synthesis, and bioactive evaluation *in vitro* and *in vivo*, *European Journal of Medicinal Chemistry* (2019), doi: <https://doi.org/10.1016/j.ejmech.2019.01.004>.

This is a PDF file of an unedited manuscript that has been accepted for publication. As a service to our customers we are providing this early version of the manuscript. The manuscript will undergo copyediting, typesetting, and review of the resulting proof before it is published in its final form. Please note that during the production process errors may be discovered which could affect the content, and all legal disclaimers that apply to the journal pertain.

Graphical Abstract



**Identification of 3-(benzazol-2-yl)quinoxaline derivatives as
potent anticancer compounds: privileged structure-based design,
synthesis, and bioactive evaluation *in vitro* and *in vivo***

Qing-Qing Liu[†], Ke Lu[†], Hai-Miao Zhu, Shi-Lin Kong, Jing-Mei Yuan, Guo-Hai Zhang,
Nan-Ying Chen, Chen-Xi Gu, Cheng-Xue Pan*, Dong-Liang Mo*, Gui-Fa Su*

State Key Laboratory for Chemistry and Molecular Engineering of Medicinal Resources, Ministry
of Science and Technology of China; School of Chemistry and Pharmaceutical Sciences, Guangxi
Normal University, 15 Yu Cai Road, Guilin 541004, China

[†]These authors contributed equally to this work.

*Corresponding Authors: Professors Cheng-Xue Pan, Dong-Liang Mo, and Gui-Fa Su
Tel. & Fax: +86 773 5826869, Email: chengxuepan@163.com (C.-X. Pan);
moeastlight@gxnu.edu.cn (D.-L. Mo); gfyglgx@163.com (G.-F. Su)

ABSTRACT

Inspired by the common structural characteristics of numerous known antitumor compounds targeting DNA or topoisomerase I, 3-(benzazol-2-yl)-quinoxaline-based scaffold was designed via the combination of two important privileged structure units—quinoxaline and benzazole. Thirty novel 3-(benzazol-2-yl)-quinoxaline derivatives were synthesized and evaluated for their biological activities. The MTT assay indicated that most compounds possessed moderate to potent antiproliferation effects against MGC-803, HepG2, A549, Hela, T-24 and WI-38 cell lines. 3-(Benzoxazol-2-yl)-2-(N-3-dimethylaminopropyl)aminoquinoxaline (**12a**) exhibited the most potent cytotoxicity, with IC₅₀ values ranging from 1.49 to 10.99 μ M against the five tested cancer and one normal cell line. Agarose-gel electrophoresis assays suggested that **12a** did not interact with intact DNA, but rather it strongly inhibited topoisomerase I (Topo I) via Topo I-mediated DNA unwinding to exert its anticancer activity. The molecular modeling study indicated that **12a** adopt a unique mode to interact with DNA and Topo I. Detailed biological study of **12a** in MGC-803 cells revealed that **12a** could arrest the cell cycle in G2 phase, inducing the generation of reactive oxygen species (ROS), the fluctuation of intracellular Ca²⁺, and the loss of mitochondrial membrane potential ($\Delta\Psi_m$). Western Blot analysis indicated that **12a**-treatment could significantly up-regulate the levels of pro-apoptosis proteins Bak, Bax, and Bim, down-regulate anti-apoptosis proteins Bcl-2 and Bcl-xl, and increase levels of cyclin B1 and CDKs inhibitor p21, cytochrome c, caspase-3, caspase-9 and their activated form in MGC-803 cells in a dose-dependent manner to induce cell apoptosis via a caspase-dependent intrinsic mitochondria-mediated pathway. Studies in MGC-803 xenograft tumors models demonstrated that **12a** could significantly reduce tumor growth *in vivo* at doses as low as 6 mg/kg with low toxicity. Its convenient preparation and potent anticancer efficacy *in vivo* makes the 3-(benzazol-2-yl)quinoxaline scaffold a promising new chemistry entity for the development of novel chemotherapeutic agents.

Keywords: Topoisomerase I inhibitor, DNA unwinding, Quinoxaline derivatives, Privileged structure, Anticancer

1. Introduction

Cancer has become the leading cause of death worldwide, especially in developing countries [1]. In 2015, there were about 4.3 million newly diagnosed cases of invasive cancer in China, leading to more than 2.8 million deaths in that year alone [2]. Thus, the investigation and identification of more effective agents to treat cancer is urgently needed.

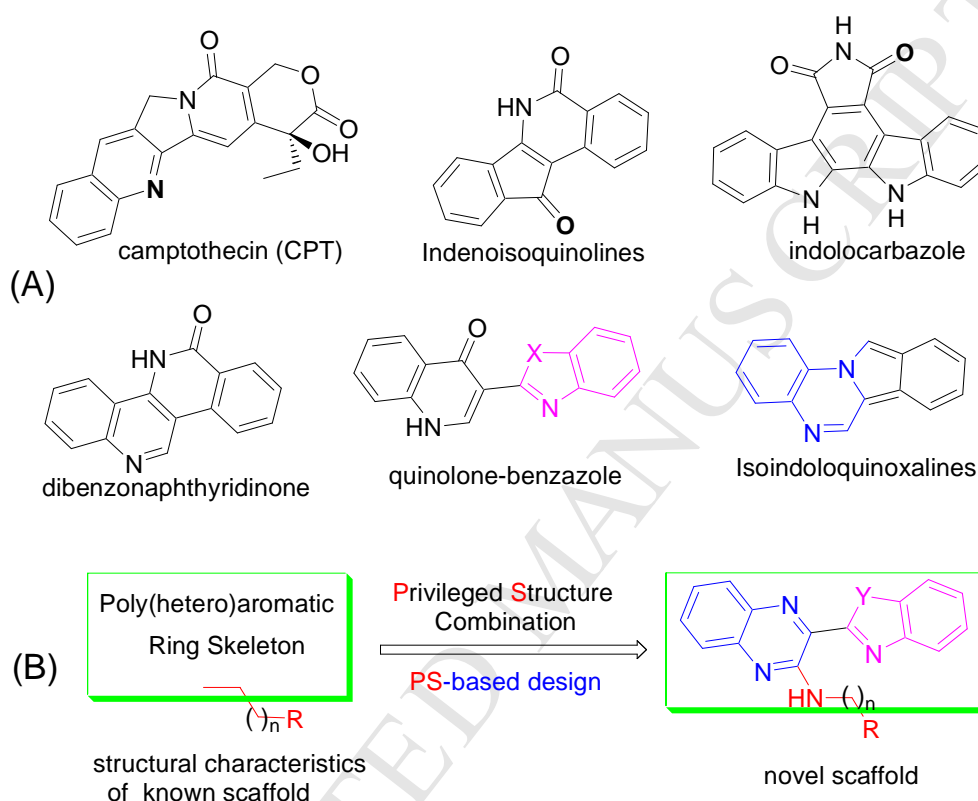


Fig. 1. Representative Topo I inhibitors and strategy to design novel scaffold

DNA and DNA Topo I are important pharmacologic targets in the development of anti-cancer therapeutics [3–5]. Topo I inhibitors are important chemotherapeutic agents. They can interfere with the Topo I through two different mechanisms, namely pensioner or catalytic inhibitor[6-9]. To date, the most intensive studies scaffold of Topo I inhibitors including the derivatives of camptothecin(CPT), indolocarbazole[7–8], dibenzonaphthyridinone[7–8], Indenoisoquinoline[9]. Some quinolone-benzazoles[10] and isoindoloquinoxalines[11] also were identified as promising Topo I inhibitors(**Fig. 1 A**).

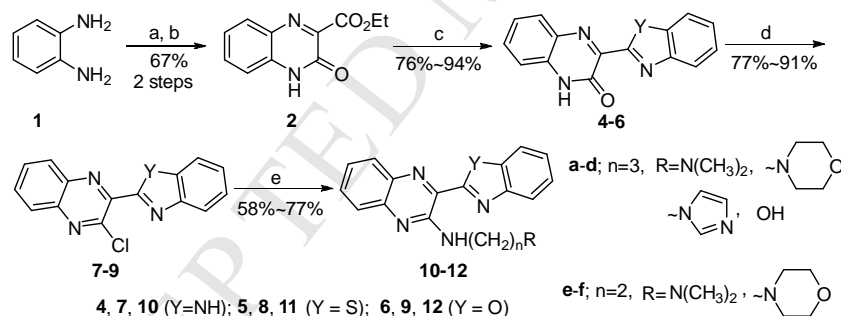
Even though Topo I inhibitors reported in literatures are very structurally diverse, most of them possess a polycyclic skeleton with a side chain that usually contain an ω -dialkyl-amino or nitrogen-containing heterocycle (**Fig. 1 B**). Considering that

drug-likeness such as ideal physicochemical and pharmacokinetic profiles, are crucial factors for drug development. And it had been well known that introduction privileged structure into the scaffold might help to improve the drug-likeness of the proposed compounds [12–13]. We envisioned that a privileged structure-based design, as depicted in Fig. 1, might serve as a useful strategy to help us to find novel anticancer scaffolds with suitable physicochemical and pharmacokinetic profiles.

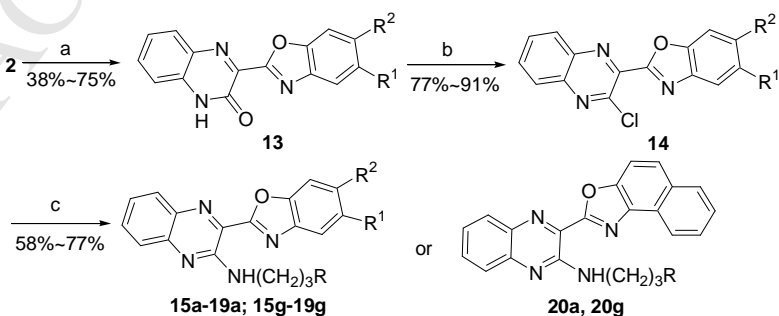
Herein, we report the design, synthesis, and bioactive evaluation of a novel anticancer scaffolds in which quinoxaline and benzazole were selected as the privileged structure motifs, since quinoxaline [14–17] and benzazole [18–32] derivatives are very important in drug development and widely present in many clinical drugs or bioactive compound. The novel scaffold also can be views as the combination of two important units of Topo I inhibitors quinolone-benzazoles and isoindoloquinoxalines reported in literature (**Fig. 1 A**).

2. Results and discussion

2.1. Chemistry



Scheme 1. Reagents and conditions: (a) $\text{CHBr}(\text{CO}_2\text{Et})_2$, 1.1 eq, EtOH, r.t.; (b) O_2 , $\text{CeCl}_3 \cdot 7\text{H}_2\text{O}$, $(\text{CH}_3)_2\text{CHOH}$, r.t.; (c) **3** (benzene-1,2-diamine, 2-amino-benzenethiol or 2-amino-phenol, 1.1 eq), Ph_2O , reflux; (d) POCl_3 , reflux; (e) $\text{R}(\text{CH}_2)_n\text{NH}_2$, toluene, 90°C



15-17: $\text{R}^1=\text{Cl}$, CH_3 , $t\text{-Bu}$; $\text{R}^2=\text{H}$; 18-19: $\text{R}^1=\text{H}$; $\text{R}^2=\text{Cl}$, CH_3 ; a: $\text{R} = \text{N}(\text{CH}_3)_2$; g: $\text{R} = \text{N}(\text{Et})_2$

Scheme 2. Reagents and conditions: (a) 1.1 eq 2-amino-phenol derivatives or 1-amino-naphthalen-2-ol, Ph_2O , reflux; (b) POCl_3 , reflux; (c) $\text{R}(\text{CH}_2)_3\text{NH}_2$, toluene, 90°C

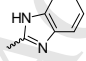
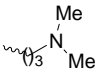
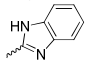
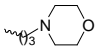
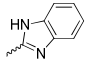
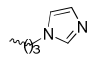
The preparation of the 3-(benzazol-2-yl)quinoxaline derivatives (**10–12**, **15–20**) was outlined in Scheme 1 and Scheme 2. Benzene-1,2-diamine **1** and diethyl 2-bromomalonate in ethanol were refluxed to give the intermediate 3-oxo-1,2,3,4-tetrahydro-quinoxaline-2-carboxylate, which was further dehydrogenated under 1 atm oxygen atmosphere promoted by cerium (IV) chloride heptahydrate to provide the 3-oxo-3,4-dihydro-quinoxaline-2-carboxylate **2**. Then **2** condensed with **3** (benzene-1,2-diamine, or 2-amino-benzenethiol, or 2-amino-phenol) in diphenyl ether to afford **4–6** in high yield. **4–6** were refluxed in excess POCl₃ to provide the 2-chloro-3-(benzazol-2-yl)quinoxaline **7–9**, followed by reacted with different amines [33] to furnish the targeted compounds **10–12** (Scheme 1). Synthesis of **15–20** was followed the same procedure as the synthesis of compounds **10–12** starting from **2** and substituted 2-amino-phenol or 1-amino-naphthalen-2-ol (Scheme 2).

2.2. Biological evaluation

2.2.1. Antiproliferative activity

The *in vitro* anti-proliferative activity of the target compound **10–12** and **15–20** against five human tumor cell lines (MGC-803, HepG-2, A549, HeLa and T24) and one normal cell (WI-38) was evaluated by the MTT assay. The IC₅₀ values derived from the dose-response curves are summarized in Table 1.

Table 1 Structures and *in vitro* cytotoxicity of compounds **10–12** and **15–20**

Cmpd	Ar	R	IC ₅₀ (μM)					
			WI-38	MGC-803	HepG2	A549	HeLa	T-24
10a			>100	26.01 ±3.85	36.45 ±4.08	67.99 ±11.1	67.54 ±9.99	60.82 ±9.04
10b			>100	>100	>100	>100	>100	>100
10c			>100	>100	>100	>100	>100	>100

10d		>100	>100	>100	>100	>100	>100
10e		14.29 ± 1.15	10.36 ± 1.02	14.17 ± 1.87	15.04 ± 1.70	69.92 ± 12.4	10.82 ± 0.98
10f		>100	>100	>100	>100	>100	>100
11a		7.41 ± 0.87	8.26 ± 0.92	11.79 ± 1.07	5.34 ± 0.73	12.55 ± 1.09	11.81 ± 1.27
11b		>100	>100	>100	>100	>100	>100
11c		>100	19.81 ± 1.90	11.67 ± 1.06	52.71 ± 8.05	39.74 ± 7.13	34.29 ± 7.17
11d		>100	>100	>100	>100	>100	>100
11e		9.74 ± 0.99	5.86 ± 0.77	12.95 ± 1.11	5.67 ± 0.75	12.65 ± 1.10	6.81 ± 0.79
11f		>100	>100	>100	>100	>100	>100
12a		10.99 ± 1.06	1.49 ± 0.18	5.27 ± 0.72	6.91 ± 0.84	6.38 ± 0.81	4.49 ± 0.65
12b		>100	>100	>100	>100	>100	>100
12c		>100	>100	>100	>100	>100	>100
12d		>100	>100	>100	>100	>100	>100
12e		6.82 ± 0.83	2.93 ± 0.47	8.52 ± 0.93	5.39 ± 0.73	15.34 ± 1.05	4.21 ± 0.62

12f			>100	>100	>100	>100	>100	>100
15a			11.09 ±1.07	8.72 ±1.13	13.83 ±1.50	11.89 ±1.52	10.01 ±0.94	5.66 ±0.23
16a			13.54 ±1.68	12.20 ±1.17	16.45 ±1.24	13.52 ±1.79	12.52 ±1.55	10.87 ±1.09
17a			14.80 ±1.04	13.87 ±1.53	>100	>100	>100	18.40 ±0.94
18a			15.33 ±1.04	14.01 ±1.21	>100	14.47 ±1.24	15.40 ±1.99	7.83 ±0.51
19a			10.95 ±0.83	8.96 ±1.55	8.82 ±0.65	8.35 ±0.41	11.98 ±0.91	5.99 ±0.22
20a			16.45 ±1.88	11.29 ±1.15	10.76 ±1.32	4.66 ±0.71	10.54 ±0.92	5.75 ±0.31
15g			11.20 ±0.01	9.20 ±1.68	13.74 ±1.62	9.32 ±1.17	10.15 ±1.36	5.49 ±0.62
16g			12.57 ±0.79	7.88 ±0.48	12.74 ±0.12	7.98 ±1.15	8.71 ±1.08	6.96 ±0.81
17g			25.15 ±3.71	10.53 ±0.83	>100	14.39 ±1.08	19.50 ±2.08	7.58 ±0.69
18g			13.57 ±1.66	11.81 ±1.77	13.47 ±1.01	12.98 ±1.18	12.51 ±1.18	9.32 ±0.99
19g			12.26 ±0.94	9.01 ±1.14	13.09 ±2.36	7.88 ±1.09	10.30 ±1.46	6.13 ±0.34
20g			14.71 ±2.36	11.51 ±2.28	12.73 ±2.36	11.34 ±2.61	10.85 ±1.02	8.00 ±0.87
CPT^b			8.37 ±0.52	2.96 ±0.23	4.79 ±0.54	4.43 ±0.85	6.51 ±0.83	6.80 ±0.54

^aResults were expressed as means \pm SD (standard deviation) from triplicate assay in a single experiment, $P < 0.05$.

^bCPT: Camptothecin

As shown in Table 1, compounds **10e**, **11a**, **11e**, **12a**, **12e** and **15–20** exhibited moderate to potent cytotoxicity against all the tested cell lines. The data indicated that the side chains at the 2-position of the quinoxaline ring played an important role in bioactivity. Only side chains with ω -dialkylamino substitution resulted in significant cytotoxic potency (series **a**, **e** and **g**), and a ω -dimethylamino substitution (series **a** and **e**) was more favorable than ω -diethylamino ones (series **g**). The length of the side chain also affected the anti-proliferative activity. The aminopropyl group (series **a**) generally yielded greater potency than the aminoethyl group (series **e**).

The benzazol group on 3-position of quinoxaline also contributed to the anti-proliferative activity of the target compound. In general, the benzoxazole gave the most potent activity (series **12**). When the benzoxazole was replaced by benzoimidazole, benzothiazole, or naphthoxazole (series **10**, **11** or **20**, respectively), the cytotoxicities of the compounds were slightly decreased.

The data in Table 1 suggested that the substituents on the benzoxazole ring and their position did not significantly impact the anti-proliferative activity of the targeted compounds. Hydrogen (H) atom (**12a**) appeared to be more favorable than any other common substituent such as halogen atoms (**15** and **18**) or alkyls (**16**, **17** and **19**). However, when the substituent was bulky, such as *t*-butyl (**17a**, **17g**), the cytotoxicity of the compounds would significant decrease.

Among the tested compound listed in table 1, **12a** not only displayed exceptional efficacy against MGC-803 cancer cell lines with IC_{50} values as low as 1.49 ± 0.18 μ M, but exhibited less toxicity ($IC_{50} = 10.99 \pm 1.06$ μ M) to normal cell WI-38 from human lung tissue. To further test the safety of compound **12a**, its cytotoxicity against normal human liver cell 7702 was further evaluated. The results indicated that **12a** also exhibit more potent cytotoxicity against cancer cell MGC-803 ($IC_{50} = 1.63 \pm 0.25$ μ M) than to normal human liver cell 7702 ($IC_{50} = 5.2 \pm 0.67$ μ M).

2.2.2. The cytotoxic compounds and **12a** did not interact with intact DNA

Since the targeted compounds were designed based on common structural characteristics of known scaffolds able to interact with DNA or DNA/topoisomerase I. To gain insight into the drug-target interaction of these novel scaffolds, we first explored whether DNA was the direct target of these compounds. DNA intercalation

of fifteen selected compounds with potent cytotoxicity were evaluated via an agarose-gel electrophoresis assay [33–34]. Ethidium bromide (EB), a well-known DNA intercalator was used as the positive control. Compared with the EB which demonstrated strong DNA intercalation activity, as indicated by its ability to induce noticeable retardation of DNA migration, the tested compounds did not result in obvious retardation of DNA migration (Fig. 2A & 2B), suggesting that the tested compounds were not directly interacting with intact DNA.

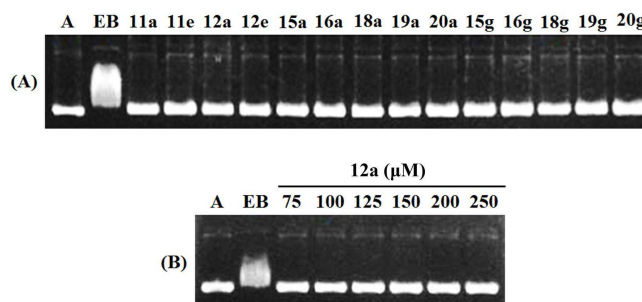


Fig. 2. (A) DNA intercalation assay of the selected compounds in 50 μ M. Lane 1(A): DMSO + DNA, lane 2: EB (10 μ M) + DNA, lanes 3–16: selected cytotoxic compounds (50 μ M, respectively) + DNA. (B) DNA intercalation assay of **12a** in different concentration. Lane 1(A): DMSO + DNA, lane 2: EB (10 μ M) + DNA, lanes 3–8: **12a** (75, 100, 125, 150, 200, 250 μ M, respectively) + DNA.

2.2.3. The cytotoxic compounds and **12a** induced potent topoisomerase I inhibition via Topo I-mediated DNA unwinding

Having determined that the tested compounds had low binding affinity with intact DNA, we then performed a topoisomerase I inhibition assay [35–37] to determine whether they acted as topoisomerase I inhibitors. The inhibitory effects of these selected compounds against Topo I was determined by measuring the migration of supercoiled plasmid DNA via agarose-gel electrophoresis, which indicated the degree of DNA relaxation. The well-known Topo I inhibitor camptothecin (CPT) was used as a positive control.

As depicted in Fig. 3A, most of the tested compounds exhibited potent Topo I inhibitory activity at 50 μ M, except for **20a** and **20g** which contain a naphthoxazole ring at the 3-position and demonstrated no apparent inhibitory activity, indicating that **20a** and **20g** might exert their cytotoxic effect via a different mechanism. The Topo I inhibitory activity of **12a**, which demonstrated the strongest cytotoxicity activity, was

further tested at concentrations from 5 to 60 μM and found that 40 μM of **12a** was sufficient to completely inhibit the activity of Topo I (Fig. 3B).

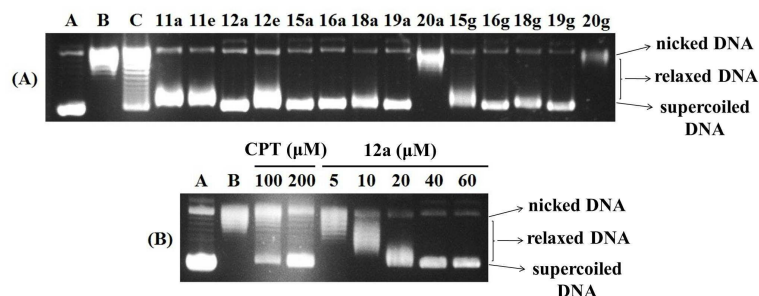


Fig. 3. (A) Topo I inhibitory activity assay of the selected compounds in 50 μM . Lane 1(A): DNA, lane 2(B): DNA + Topo I, lane 3(C): CPT (100 μM) + DNA + Topo I, lanes 4–17: selected cytotoxic compounds (50 μM , respectively) + DNA + Topo I. (B) Topo I inhibitory activity assay of the **12a** in different concentration. Lane 1(A): DNA, lane 2(B): DNA + Topo I, lanes 3–4: CPT (100, 200 μM , respectively) + DNA + Topo I, lanes 5–9: **12a** (5, 10, 20, 40, 60 μM , respectively) + DNA + Topo I.

By comparison with the bands in Fig. 3, it could be determined that the Topo I inhibition mode of the tested compounds was different to that of the positive control CPT, a Topo I inhibitor acting by forming a drug-enzyme-DNA ternary complex [6] and cleaving DNA, which was indicated by the production of nicked DNA in the CPT bands.

According to the catalytic cycle of Topo I [5], DNA intercalating or unwinding agents also could inhibit Topo I by unwinding closed circular DNA [38]. To gain further insight into the Topo I inhibition mechanism of the 3-(benzazol-2-yl)quinoxaline derivatives, we investigated whether they could produce DNA unwinding in the presence of excess Topo I. EB, a DNA intercalating agent, was used as a positive control, and CPT, which inhibits Topo I by forming the drug-enzyme-DNA covalent ternary complex, was used as a negative control.

As shown in Fig. 4A, EB and most of the tested 3-(benzazol-2-yl)-quinoxaline derivatives exhibited clear DNA unwinding at 50 μM , except for compounds **20a** and **20g** which demonstrated no Topo I inhibitory activity. The most cytotoxic compound **12a** was further tested at concentrations from 5 to 60 μM . We found that **12a** could exert its significant Topo I-mediated unwinding effect at 20 μM (Fig. 4B), indicating that **12a** exerts its Topo I inhibitory activity via Topo I-mediated DNA unwinding.

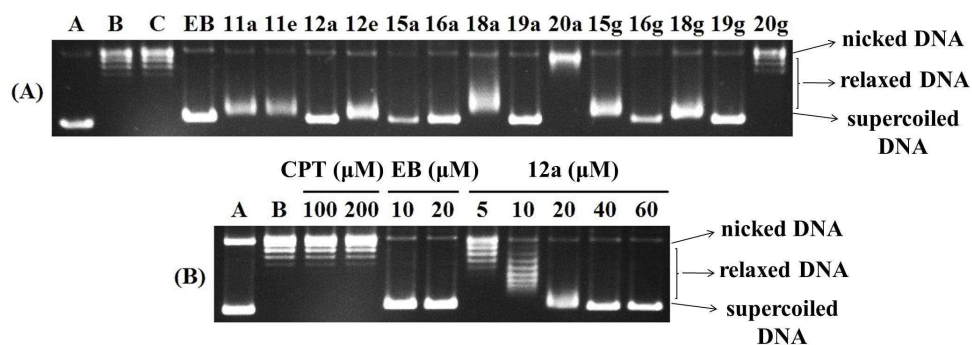


Fig. 4. (A) Topo I inhibitory activity assay of the selected compounds in 50 μ M. Lane 1(A): DNA, lane 2(B): DNA + Topo I, lane 3(C): CPT (100 μ M) + DNA + Topo I, lane 4: EB (50 μ M) + DNA + Topo I, lanes 5–18: selected compounds (50 μ M, respectively) + DNA + Topo I. (B) Lane 1(A): DNA, lane 2(B): DNA + Topo I, lanes 3–4: CPT (100, 200 μ M, respectively) + DNA + Topo I, lanes 5–6: EB (10, 20 μ M, respectively) + DNA + Topo I, lanes 7–11: **12a** (5, 10, 20, 40, 60 μ M, respectively) + DNA + Topo I.

2.2.4. Molecular modeling

Since the mechanism studies indicated that **12a** might blocks the combination between DNA and Topo I via Topo I-mediated DNA unwinding, a molecular docking study was performed using C-DOCKER in Discovery Studio 2017R2 to predict and to better understand the binding mode of **12a** with DNA and Topo I. The structure of the ternary complex, containing topoisomerase I, DNA, and CPT, was downloaded from the Protein Data Bank (PDB code 1T8I).

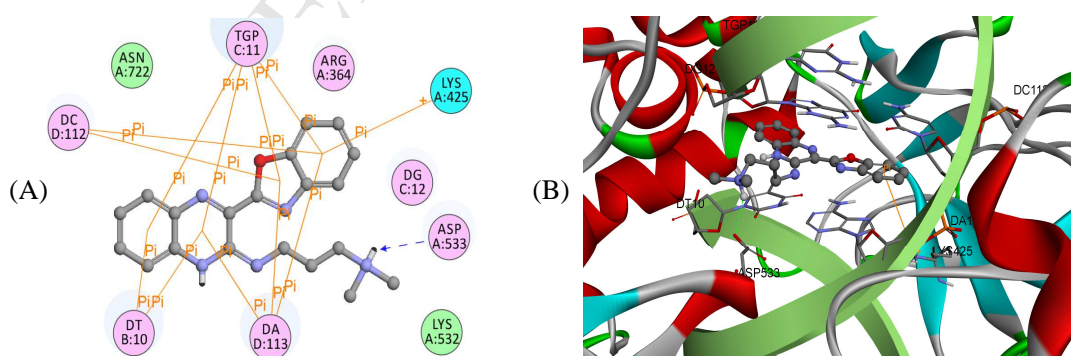


Fig. 5. The 2D(A) and 3D(B) diagram of hypothetical binding mode for **12a** with DNA-Topo I.

As shown in Fig. 5A and B, The docking results suggest that **12a** binds with the DNA-Topo I complex in a unsimilar manner to that of the Topo I poisoner [39] or the

Topo I catalytic inhibitor [40]. In the **12a** -DNA-Topo I ternary complex. The dimethyl amino group on the side chain was protonation and hydrogen bonding to ASP533 in Topo I, while the quinoxaline and benzoxazole ring interact by pi-pi interaction through the insertion of planar aromatic rings between DNA base pairs. The electron-rich nature of the benzoxazole ring also furnish it to interact with LYS425 via pi-cation interaction.

The results provide evidence for the mechanism with which **12a** interfere with the Topo I/DNA. The non-coplanar feature of the quinoxaline and benzoxazole ring make this scaffold not easily direct intercalate into intact DNA. But if the supercoiled DNA was relaxed by Topo I, the compounds will be able to insert into DNA and interact with Topo I/DNA. The results also well explain how the length and the ω -substituent of the side chain, as well as the bulk of substituents on the aryl ring affect the activities of the target compounds.

2.2.5. Compound **12a** induced G2 phase cell cycle arrest

As **12a** displayed the most promising activity not only in cytotoxicity but also in Topo I inhibition, the mechanism of its cytotoxic effect was further studied. Whether **12a** inhibited the proliferation of MGC-803 cells through cell cycle arrest was first examined by flow cytometry. As shown in Fig. 5, **12a** treatment (doses from 0, 1.0, 2.0 to 8.0 μ M, 48 h) clearly increased the proportion of cells in G2 phase from 3.77%, 8.09%, 11.67%, to 26.09%, whereas the S phase population decreased from 41.88% in the control to 25.65% (8.0 μ M). These results indicated that **12a** caused G2 arrest in a dose-dependent manner and that its anti-proliferation in cancer cell lines was potentially due to G2 phase arrest.

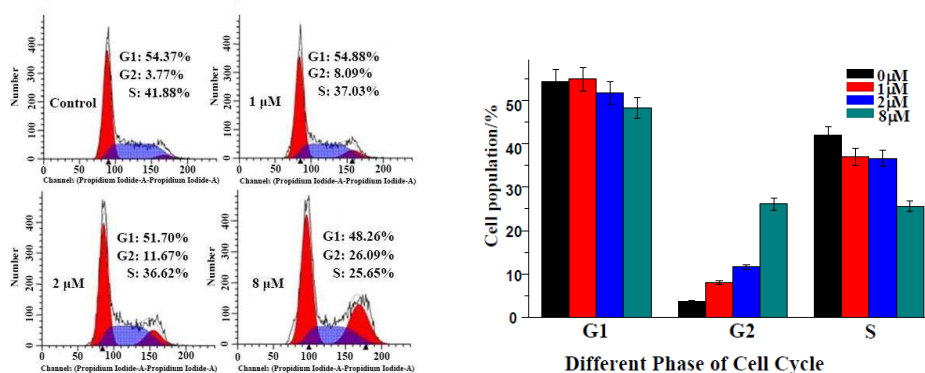


Fig. 5. Cell cycle analysis of compound **12a** in MGC-803 cells. Cells were treated with **12a** (0, 1.0, 2.0 and 8.0 μ M, respectively) for 48 h.

The formation of cyclin B1-CDK1 complexes is required for the cell cycle transition from G2 to M phase during cell division [41]. To further confirm the G2 cell cycle arrest caused by **12a**, we investigated the levels of Cyclin B1 and cyclin-dependent kinase (CDK) inhibitor p21 in MGC-803 cells. Immunoblotting assay revealed that **12a**-treatment would increase the amount of Cyclin B1 and p21 in MGC-803 cells (Fig. 6), suggesting that **12a** might not only could up-regulate the levels of CDK inhibitor p21, but also hinder cyclin B1 binding to CDK1 to form the cyclin B1-CDK1 complex, resulting in G2 arrest induced by **12a**.

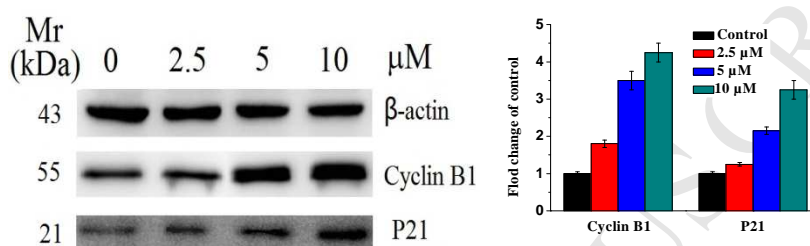


Fig. 6. Effect of **12a** on the level of Cyclin B1 and CDK inhibitor p21 in cell detected by western blot. Protein was from MGC-803 cell line treated by **12a** (0, 2.5, 5.0 and 10 μ M, respectively) for 24 h. Whole-cell extracts were prepared and analyzed using antibodies against proteins indicated. The data are representative of three independent experiments. * $P < 0.05$, ** $P < 0.01$, *** $P < 0.001$ vs the negative control.

2.2.6. Compound **12a** induced cell apoptosis via caspase-dependent intrinsic mitochondrial pathway

To further examine whether the observed cytotoxicity was due to induction of apoptosis, Annexin V FITC/PI dual staining assay was performed to evaluate the apoptosis-inducing effect of **12a**. MGC-803 cells were treated with **12a** at a dose of 0, 2.5, 5.0, 10.0 μ M for 24 h. As shown in Fig. 7, the percentage of apoptotic cells was increased from 1.82% (0 μ M) to 10.77% (2.5 μ M), 17.94% (5.0 μ M) and 26.38% (10.0 μ M), respectively, indicating that **12a** could induce MGC-803 cell apoptosis in a dose-dependent manner.

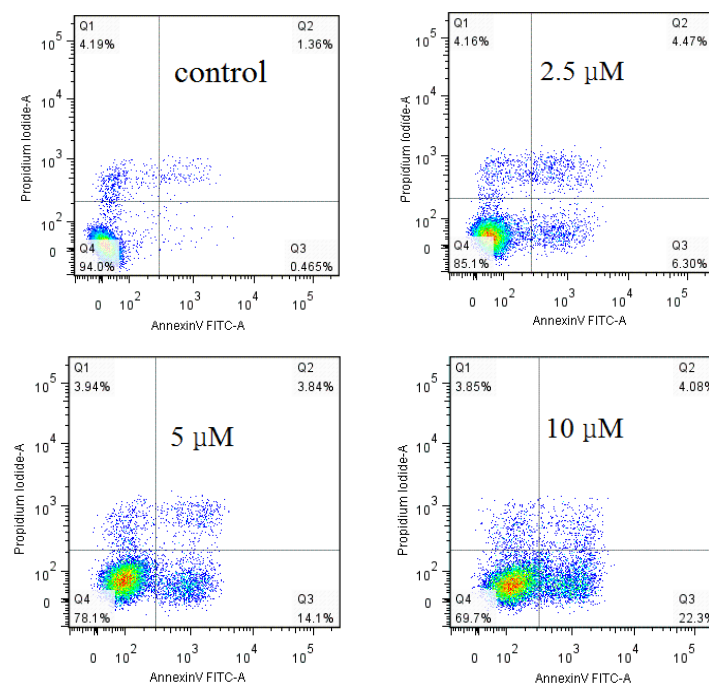


Fig. 7. The induction of apoptosis effects of **12a** in MGC-803 cells. Cell was treated with **12a** (0, 2.5, 5.0 and 10 μ M, respectively) for 24 h and the results were examined by FACS analysis with PI and FITC-Annexin V staining.

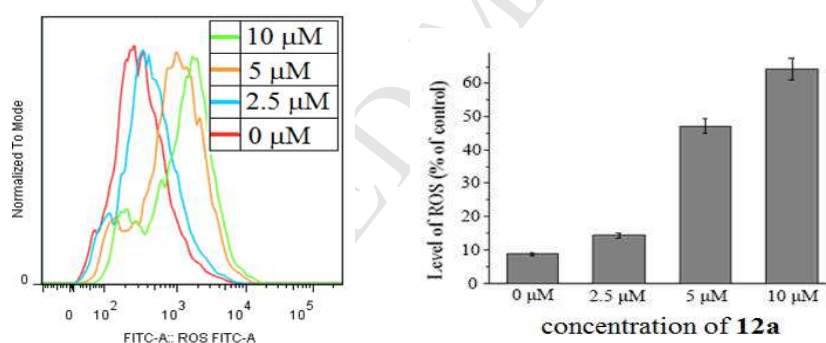


Fig. 8. ROS generation assay of compound **12a** in MGC-803 cells. MGC-803 cells were treated with **12a** (0, 2.5, 5.0 and 10 μ M, respectively) for 24 h.

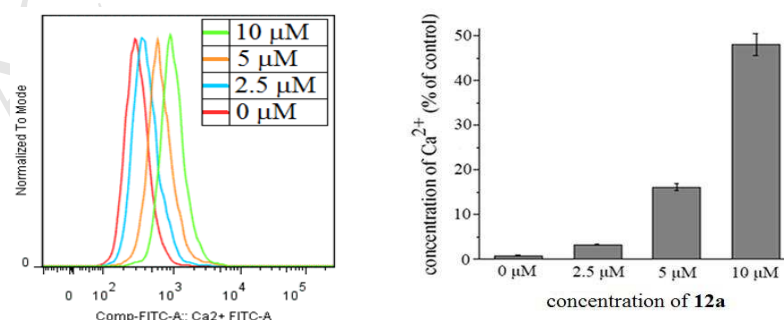


Fig. 9. Effect of **12a** on intracellular Ca²⁺ level in MGC-803 cells. MGC-803 cells were treated with **12a** (0, 2.5, 5.0 and 10 μ M, respectively) for 24 h.

As reactive oxygen species (ROS) [42] and Ca^{2+} [43–44] play key roles in the regulation of apoptosis, to determine whether **12a** treatment would induce the production of ROS and fluctuation of Ca^{2+} , MGC-803 cells were treated with **12a** at doses from 0, 2.5, 5.0 to 10.0 μM for 24 h in the presence of 2',7'-dichloro-fluorescein (DCF) or fura-3 AM, which are fluorescent indicators for ROS and Ca^{2+} , respectively.

As depicted in Fig. 8 and Fig. 9, the fluorescence intensities were significantly increased when the dose of **12a** increased, indicating that intracellular ROS and Ca^{2+} levels increased in a dose-dependent manner after **12a**-treatment, which may be responsible for apoptosis induction by **12a**.

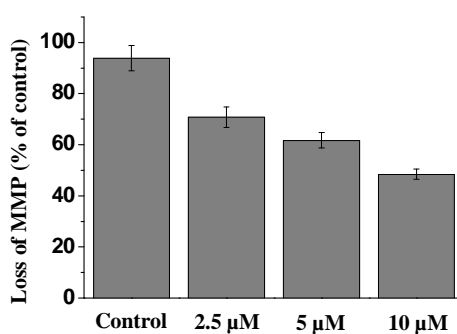
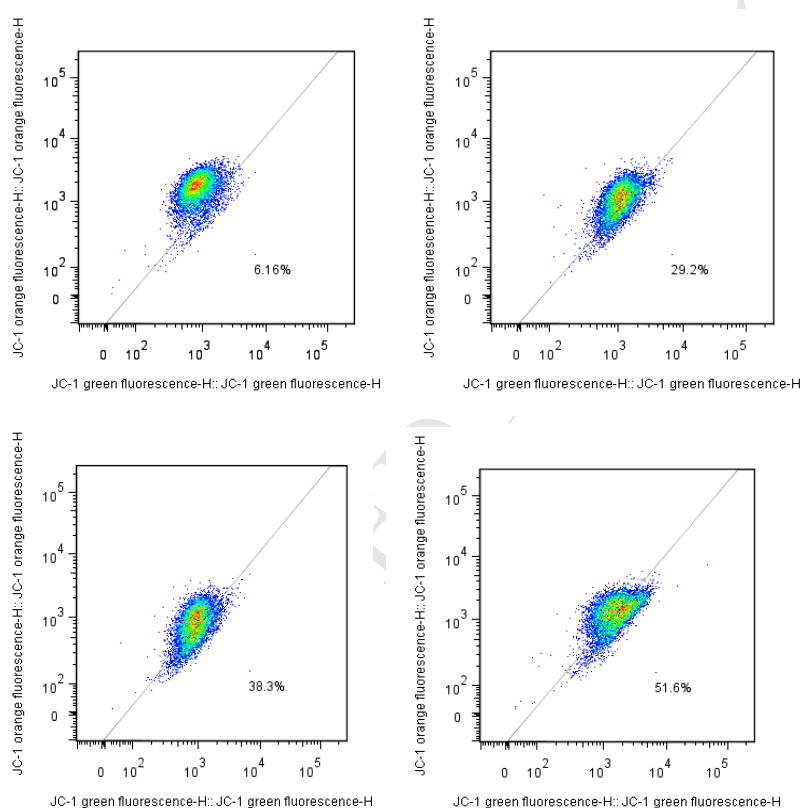


Fig. 10. Effect of **12a** on $\Delta\Psi_m$ of MGC-803 cells. MGC-803 cells were treated with **12a** (0, 2.5, 5.0 and 10 μ M, respectively) for 24 h.

To further determine the pathway that mediated the induction of cell apoptosis by **12a**, the mitochondrial membrane potential ($\Delta\Psi_m$) of **12a**-treated MGC-803 cells was measured by the fluorescent probe JC-1 (5,5',6,6'-tetrachloro-1,1',3,3'-tetraethylbenzimidazolylcarbocyanine). As shown in Fig. 10, the fluorescence intensity in MGC-803 cells was obviously decreased after treatment with **12a** (doses 0, 2.5, 5.0, 10.0 μ M) for 24 h, especially when the dose of **12a** was increased from 0 to 2.5 μ M, suggesting that the **12a**-treatment could result in the loss of $\Delta\Psi_m$ that usually indicate the mitochondrial dysfunction associated with intrinsic mitochondrial apoptosis pathway [45].

In order to get more detailed information about the apoptotic-induction of **12a**, the levels of apoptosis-related Bcl-2 family proteins which are regarded as key regulators of cell apoptosis [46–47], and the indicators of activation of the mitochondrial apoptosis pathway [48–49], such as cytochrome c, caspase-9, caspase-3 and their cleaved forms were measured by Western blot.

As shown in Fig. 11, the expression of anti-apoptosis proteins Bcl-2 and Bcl-xl, especially the later, were obviously down-regulated, whereas the expression of pro-apoptotic proteins Bak, Bax and Bim were up-regulated, confirming that apoptosis was induced by **12a**. Meanwhile, the level of cytochrome c, caspase-3 and caspase-9, and the cleaved form of these proteins in the tumor cell were increased significantly after **12a**-treatment (Fig. 12), indicating that **12a** induced cell apoptosis via a caspase-dependent intrinsic mitochondria-mediated pathway.

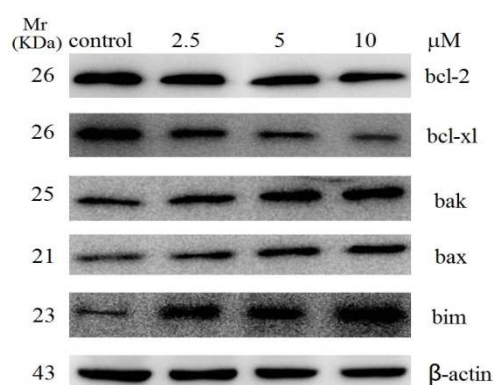


Fig. 11. Effect of **12a** on the level of Bcl-2, Bcl-xl, Bak, Bax and Bim in cell detected by Western blot. Protein was from MGC-803 cell line treated by **12a** (0, 2.5, 5.0 and 10 μ M, respectively) for

24 h. Whole-cell extracts were prepared and analyzed using antibodies against proteins indicated. β -Actin was used as a loading control. The data are representative of three independent experiments. * $P < 0.05$, ** $P < 0.01$, *** $P < 0.001$ vs the negative control.

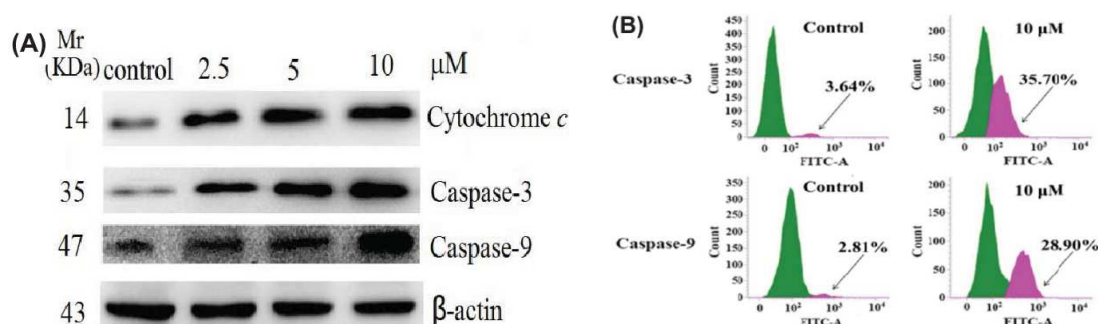


Fig. 12. (A) Effect of **12a** on the level of cytochrome c, caspase-3/9 in cell detected by Western blot. Protein was from MGC-803 cell line treated by **12a** (0, 2.5, 5.0 and 10 μ M, respectively) for 24 h. (B) **12a** induced apoptosis by triggering Caspase-3, Caspase-9 activities in MGC-803 cells. MGC-803 cells were incubated with 10 μ M of **12a** for 24 h. Arrow showed the Caspase-3 or Caspase-9 activated cells.

2.2.7. Compound **12a** demonstrated potential anticancer potency *in vivo* with low toxicity

The *in vivo* anticancer efficiency of **12a** was further evaluated using MGC-803 xenograft tumors models. Twenty-four nude mice with tumors at a volume of 80–200 mm³ were randomized to vehicle, CPT-treatment (6 mg/kg/2 days), low dose **12a**-treatment (6 mg/kg/2 days), and high dose **12a**-treatment (12 mg/kg/2 days) groups (6 mice/group). The treatment groups were ip injection every other day of CPT or **12a**. As shown in Fig. 13a, b, d, as compared with the vehicle control group, the *in vivo* tumor growth inhibition (TGI) of **12a** was 41.0% (high doses), only 10% lower than that of CPT (51.5%). This confirmed that **12a** possessed significant tumor growth inhibition *in vivo*. The potential toxicity of **12a** was also investigated by monitoring the weight loss of all tested nude mice. As depicted in Fig. 13c, no differences were found between the vehicle control and the **12a**-treated group in body weight loss, suggesting that **12a** at the therapeutic dosage does not possess apparent toxicity.

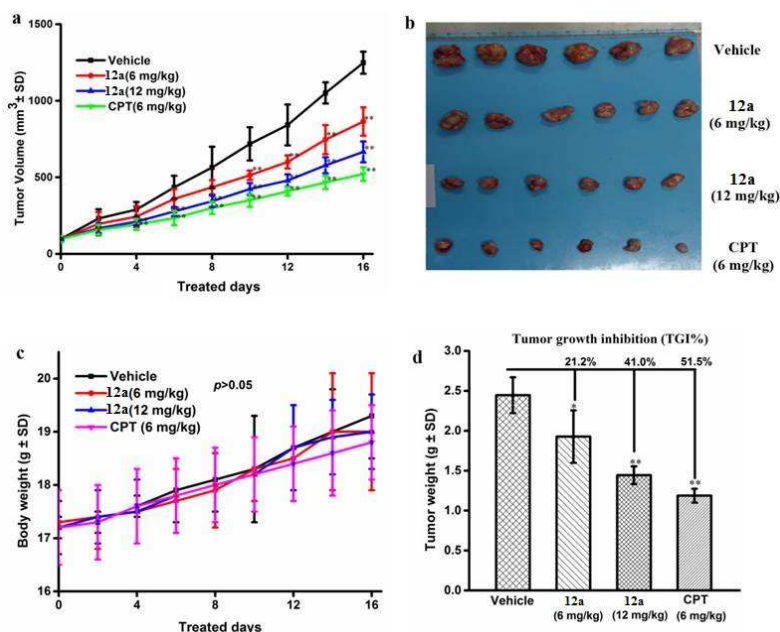


Fig. 13. *In vivo* anticancer activity of **12a** in MGC-830 xenograft mice. (a) The tumor volume of mice from each group during the observation period. Tumor-bearing mice were administered the vehicle (negative control), **12a** (6 or 12 mg/kg per 2 days) or CPT (6 mg/kg per 2 days, positive control). (b) Images of the excised tumors from each group. (c) Body weights of the mice recorded at the end of the treatments. (d) Weight of the excised tumors from MGC-830 xenograft model. Data are presented as the mean \pm SD. Error bars represent SD, $n = 6$, * $p < 0.05$ and ** $p < 0.01$, vs control.

3. Conclusion

In summary, based on the privileged structure combination, 30 novel 3-(benzazol-2-yl)quinoxaline derivatives were designed, synthesized, and studied for their cytotoxicities. The result indicated that many target compounds display potent anticancer activity *in vitro*. Agarose-gel electrophoresis assay and molecular docking indicated that most of the cytotoxic compounds could strongly inhibit Topo I activity *via* Topo I-mediated DNA unwinding. The most potent molecule, 3-(benzo[d]oxazol-2-yl)-2-(*N*-3-dimethylaminopropyl)aminoquinoxalin **12a**, was selected for further evaluation of its bioactivity. The results indicated that **12a**-treatment would increase the levels of CDK inhibitor p21 and trigger a G2 phase cell cycle arrest, induce the generation of reactive oxygen species (ROS), cause fluctuation of intracellular Ca^{2+} , loss of mitochondrial membrane potential ($\Delta\psi_m$), up-regulation the pro-apoptosis proteins Bak, Bax and Bim, down-regulation the anti-apoptosis proteins Bcl-2 and

Bcl-xl, increases the level of cytochrome c, caspase-3 and caspase-9 and their activated forms in MGC-803 cells in a dose-dependent manner, and finally triggering a caspase-dependent intrinsic mitochondria-mediated cell apoptosis. Compound **12a** also demonstrated potent anticancer efficiency *in vivo* with low toxicity and could be served as a promising lead compound for further drug development.

4. Experimental section

4.1. Chemistry

All reagents were purchased from commercial sources and were used without further purification. Melting points were recorded on a X-5 apparatus without correction. NMR spectra were recorded in CDCl₃ or in DMSO-*d*₆ on a Bruker Advance (500 or 400 MHz) with TMS as the internal standard. HRMS were measured in ESI mode and the mass analyzer was TOF.

4.1.1. Synthesis of ethyl 3-oxo-3,4-dihydroquinoxaline-2-carboxylate (**2**).

The solution of benzene-1,2-diamine (1.09 g, 10 mmol) and diethyl 2-bromo-malonate (1.9 mL, 11 mmol) in ethanol (20 mL) was stirred at room temperature for 4 h until the reaction completed (monitored by TLC). Then the solvent was evaporated under reduced pressure, washed with petroleum ether (10 mL × 3) to give a pale-yellow solid. The solid was dissolved in 100 mL of isopropanol, cerium trichloride heptahydrate (1.86 g, 5 mmol) and water (0.5 mL) were added and the mixture was stirred under 1 atm oxygen at room temperature for 6 h until the reaction completed (monitored by TLC). The solvent was evaporated under reduced pressure and the solid was washed with water (10 mL × 3) to provide a yellow solid **2** (2.86 g), yield 67%, mp 175–177 °C, which was used in next steps without further purification.

4.1.2. General Procedure for Synthesis of **4–6** and **13**.

Compound **2** (2.18 g, 10 mmol) and benzene-1,2-diamine (1.30 g, 12 mmol) in Ph₂O (10 mL) was heated to reflux for 2 h until the reaction completed (monitored by TLC). Then the mixture was cooled, filtered, and the solid was washed with

petroleum ether (15 mL \times 3) to give 2.28 g of grey solid **4**, which was used in next step without further purification. Compounds **5–6** and **13** were synthesized followed the same procedure.

4.1.3. General Procedure for Synthesis of **7–9** and **14**.

The mixture of compound **4** (0.52 g, 2 mmol) and redistilled POCl₃ (5 mL) was heated in 90 °C for about 2 h under nitrogen atmosphere. After completion (monitored by TLC), the excess POCl₃ was removed under reduced pressure and ice-water was poured in. The solid was filtered and washed with water. The dry crude product was further purified by column chromatography on silica gel eluted with ethyl acetate/petroleum ether (V: V = 1:8) to afford pale-yellow solid **7** (0.49 g), yield 88%, mp 216–218 °C. Compounds **8–9** and **14** were synthesized followed the same procedure.

4.1.4. Preparation of compounds **10–12** and **15–20**.

4.1.4.1. General procedure

A solution of compounds **7** (or **8** or **9** or **14**) (0.5 mmol) and amine derivatives (2.5 mmol) in toluene (5 mL) was heated in 90 °C for 1.5 h until the reaction completed (monitored by TLC). Then the solvent was removed under reduced pressure and the residue was purified by column chromatography on silica gel eluted with ethyl acetate/petroleum ether to provide **10–12** or **15–20**.

4.1.4.2. 3-(1*H*-Benzo[d]imidazol-2-yl)-2-(*N*-3-dimethylaminopropyl)aminoquin-oxaline (**10a**), 0.14 g, yield 92%, pale yellow solid, m.p. 175–176 °C, ¹H NMR (500 MHz, DMSO-*d*₆) δ 13.39 (s, 1H), 9.87 (t, *J* = 5.4 Hz, 1H), 7.94 (dd, *J* = 8.5, 0.8 Hz, 1H), 7.73–7.62 (m, 4H), 7.45–7.42 (m, 1H), 7.34 (s, 2H), 3.71–3.67 (m, 2H), 2.41 (t, *J* = 6.9 Hz, 2H), 2.20 (s, 6H), 1.89–1.83 (m, 2H). ¹³C NMR (125 MHz, DMSO-*d*₆) δ 150.8, 149.8, 142.7, 135.6, 132.7, 131.3, 128.9, 126.1, 124.7, 57.3, 45.7, 38.9, 26.9. HRMS (ESI) *m/z* calcd for C₂₀H₂₃N₆ [M+H]⁺ 347.1984, found 347.1986.

4.1.4.3. 3-(1*H*-Benzo[d]imidazol-2-yl)-2-(*N*-3-morpholino-4-ylpropyl)aminoquin-oxaline (**10b**), 0.176 g, yield 91%, yellow solid, m.p. 210–211 °C, ¹H NMR (400 MHz, DMSO-*d*₆) δ 13.40 (s, 1H), 9.84 (t, *J* = 3.6 Hz, 1H), 7.94 (d, *J* = 5.4 Hz, 1H), 7.79 (d, *J* = 5.3 Hz, 1H), 7.66–7.63 (m, 3H), 7.45–7.41 (m, 1H), 7.38–7.35 (m, 1H),

7.30 (t, $J = 5.1$ Hz, 1H), 3.71–3.68 (m, 2H), 3.59 (t, $J = 3.0$ Hz, 4H), 2.46 (t, $J = 4.6$ Hz, 2H), 2.40 (s, 4H), 1.91–1.86 (m, 2H). ^{13}C NMR (100 MHz, DMSO- d_6) δ 150.8, 149.8, 143.1, 142.6, 135.7, 134.6, 132.7, 131.3, 128.9, 126.1, 124.9, 124.7, 123.1, 119.9, 112.8, 66.7, 56.4, 53.9, 38.9, 25.8. HRMS (ESI) m/z calcd for $\text{C}_{22}\text{H}_{25}\text{N}_6\text{O}$ $[\text{M}+\text{H}]^+$ 389.2090, found 389.2075.

4.1.4.4. 3-(1H-benzo[d]imidazol-2-yl)-2-(N-3-(1H-Imidazol-1-yl)propyl)aminoquin-oxaline (**10c**), 0.165 g, yield 89%, pale yellow solid, m.p. 205–206 °C, ^1H NMR (500 MHz, DMSO- d_6) δ 13.47 (s, 1H), 9.89 (t, $J = 5.6$ Hz, 1H), 7.95 (d, $J = 8.1$ Hz, 1H), 7.73 (s, 1H), 7.65–7.63 (m, 4H), 7.47–7.43 (m, 1H), 7.28 (s, 1H), 7.02 (s, 2H), 6.94 (s, 1H), 4.16 (t, $J = 6.9$ Hz, 2H), 3.64–3.61 (m, 2H), 2.23–2.20 (m, 2H). ^{13}C NMR (125 MHz, DMSO- d_6) δ 150.7, 149.8, 143.1, 142.4, 137.8, 135.8, 135.6, 134.6, 132.7, 131.3, 128.9, 126.2, 125.0, 124.9, 123.1, 120.0, 119.8, 112.8, 44.4, 38.0, 30.6. HRMS (ESI) m/z calcd for $\text{C}_{21}\text{H}_{20}\text{N}_7$ $[\text{M}+\text{H}]^+$ 370.1780, found 370.1767.

4.1.4.5. 3-(3-(1H-Benzo[d]imidazol-2-yl)-2-(N-3-hydroxylpropyl)aminoquinoxaline (**10d**), 0.147 g, yield 92%, pale yellow solid, m.p. 208–209 °C, ^1H NMR (400 MHz, DMSO- d_6) δ 13.39 (s, 1H), 9.86 (t, $J = 3.6$ Hz, 1H), 7.95–7.93 (m, 1H), 7.83 (d, $J = 5.4$ Hz, 1H), 7.67–7.62 (m, 3H), 7.45–7.42 (m, 1H), 7.38–7.35 (m, 1H), 7.32–7.29 (m, 1H), 4.66 (t, $J = 3.4$ Hz, 1H), 3.75–3.71 (m, 2H), 3.65–3.62 (m, 2H), 1.94–1.90 (m, 2H). ^{13}C NMR (100 MHz, DMSO- d_6) δ 150.8, 149.8, 143.1, 142.6, 135.7, 134.5, 132.7, 131.3, 128.9, 126.1, 124.9, 124.7, 123.0, 120.0, 112.8, 59.1, 38.1, 32.5. HRMS (ESI) m/z calcd for $\text{C}_{18}\text{H}_{18}\text{N}_5\text{O}$ $[\text{M}+\text{H}]^+$ 320.1511, found 320.1497.

4.1.4.6. 3-(1H-Benzo[d]imidazol-2-yl)-2-(N-2-dimethylaminoethyl)aminoquinoxaline (**10e**), 0.136 g, yield 82%, pale yellow solid, m.p. 164–165 °C, ^1H NMR (400 MHz, DMSO- d_6) δ 13.36 (s, 1H), 9.96 (t, $J = 3.4$ Hz, 1H), 7.94 (d, $J = 5.3$ Hz, 1H), 7.78 (d, $J = 4.9$ Hz, 1H), 7.66–7.62 (m, 3H), 7.45–7.42 (m, 1H), 7.36 (d, $J = 4.3$ Hz, 1H), 7.31 (d, $J = 4.8$ Hz, 1H), 3.74–3.71 (m, 2H), 2.64 (t, $J = 8.4$ Hz, 2H), 2.30 (s, 6H). ^{13}C NMR (100 MHz, DMSO- d_6) δ 150.7, 149.7, 143.1, 142.6, 135.7, 134.6, 132.7, 131.2, 128.9, 126.1, 124.9, 124.7, 123.0, 120.0, 112.8, 58.2, 45.8, 39.1. HRMS (ESI) m/z calcd for $\text{C}_{19}\text{H}_{21}\text{N}_6$ $[\text{M}+\text{H}]^+$ 333.1827, found 333.1811.

4.1.4.7. 3-(1H-Benzo[d]imidazol-2-yl)-2-(N-2-morpholino-4-ylethyl)aminoquin-

-oxaline (**10f**), 0.179 g, yield 96%, pale yellow solid, m.p. 257–258 °C, ^1H NMR (400 MHz, DMSO- d_6) δ 13.36 (s, 1H), 10.05 (t, J = 3.2 Hz, 1H), 7.94 (d, J = 5.4 Hz, 1H), 7.80 (d, J = 5.3 Hz, 1H), 7.67–7.63 (m, 3H), 7.45–7.43 (m, 1H), 7.38–7.36 (m, 1H), 7.34–7.31 (m, 1H), 3.78–3.75 (m, 2H), 3.71 (t, J = 3.0 Hz, 4H), 2.70 (t, J = 4.1 Hz, 2H), 2.55 (s, 4H). ^{13}C NMR (100 MHz, DMSO- d_6) δ 150.7, 149.8, 143.2, 142.6, 134.6, 131.2, 128.9, 126.1, 124.9, 124.7, 123.0, 119.8, 112.8, 67.0, 56.8, 53.6, 37.9. HRMS (ESI) m/z calcd for $\text{C}_{21}\text{H}_{23}\text{N}_6\text{O}$ $[\text{M}+\text{H}]^+$ 375.1933, found 375.1917.

4.1.4.8. 3-(Benzo[d]thiazol-2-yl)-2-(N-3-dimethylaminopropyl)aminoquinoxaline (**IIa**), 0.117 g, yield 81%, pale yellow solid, m.p. 134–135 °C, ^1H NMR (400 MHz, DMSO- d_6) δ 9.28 (t, J = 5.4 Hz, 1H), 8.18 (t, J = 7.8 Hz, 2H), 7.87–7.86 (m, 1H), 7.68–7.60 (m, 3H), 7.57–7.54 (m, 1H), 7.44–7.41 (m, 1H), 3.73–3.69 (m, 2H), 2.66 (t, J = 6.9 Hz, 2H), 2.38 (s, 6H), 1.99–1.94 (m, 2H). ^{13}C NMR (100 MHz, DMSO- d_6) δ 169.2, 153.4, 149.9, 143.0, 135.7, 135.2, 134.5, 132.2, 129.2, 127.4, 127.3, 126.2, 125.2, 124.0, 122.9, 56.5, 44.5, 40.5, 38.8, 25.8. HRMS (ESI) calcd for $\text{C}_{20}\text{H}_{22}\text{N}_5\text{S}$ $[\text{M}+\text{H}]^+$ 364.1596, found 364.1584.

4.1.4.9. 3-(Benzo[d]thiazol-2-yl)-2-(N-3-morpholino-4-ylpropyl)aminoquinoxaline (**IIb**), 0.197 g, yield 97%, pale yellow solid, m.p. 137–138 °C, ^1H NMR (400 MHz, DMSO- d_6) δ 9.23 (t, J = 5.3 Hz, 1H), 8.20–8.13 (m, 2H), 7.86 (d, J = 8.2 Hz, 1H), 7.69–7.54 (m, 4H), 7.44–7.40 (m, 1H), 3.72–3.67 (m, 2H), 3.58 (t, J = 4.4 Hz, 4H), 2.47–2.44 (m, 2H), 2.40 (s, 4H), 1.93–1.86 (m, 2H). ^{13}C NMR (100 MHz, DMSO- d_6) δ 169.3, 153.3, 149.9, 143.1, 135.7, 135.2, 134.5, 132.3, 129.2, 127.4, 127.3, 126.1, 125.2, 123.9, 122.9, 66.7, 56.4, 53.9, 39.1, 25.7. HRMS (ESI) m/z calcd for $\text{C}_{22}\text{H}_{24}\text{N}_5\text{OS}$ $[\text{M}+\text{H}]^+$ 406.1701, found 406.1686.

4.1.4.10. 3-(Benzo[d]thiazol-2-yl)-2-(N-3-(1H-Imidazol-1-ylpropyl)aminoquinoxaline (**IIc**), 0.187 g, yield 97%, pale yellow solid, m.p. 145–146 °C, ^1H NMR (400 MHz, DMSO- d_6) δ 9.22 (t, J = 3.6 Hz, 1H), 8.17 (t, J = 5.4 Hz, 2H), 7.85 (dd, J = 5.5, 0.7 Hz, 1H), 7.71 (s, 1H), 7.67–7.64 (m, 1H), 7.62–7.58 (m, 2H), 7.55–7.52 (m, 1H), 7.42–7.40 (m, 1H), 7.27 (t, J = 0.7 Hz, 1H), 6.93 (s, 1H), 4.15 (t, J = 4.6 Hz, 2H), 3.62–3.59 (m, 2H), 2.23–2.19 (m, 2H). ^{13}C NMR (100 MHz, DMSO- d_6) δ 169.2, 153.3, 149.8, 142.9, 137.8, 135.8, 135.2, 134.5, 132.2, 129.1, 128.9, 127.3, 127.2, 126.1, 125.2, 124.1, 122.8, 119.8, 44.4, 38.1, 30.4. HRMS (ESI) m/z calcd for

$\text{C}_{21}\text{H}_{19}\text{N}_6\text{S}$ $[\text{M}+\text{H}]^+$ 387.1392, found 387.1373.

4.1.4.11. 3-(3-(Benzo[d]thiazol-2-yl)-2-(N-3-hydroxylpropyl)aminoquinoxaline (**11d**), 0.151 g, yield 90%, yellow solid, m.p. 178–179 °C, ^1H NMR (400 MHz, $\text{DMSO}-d_6$) δ 9.37 (t, $J = 3.4$ Hz, 1H), 8.18 (t, $J = 5.8$ Hz, 2H), 7.87 (d, $J = 5.4$ Hz, 1H), 7.68–7.63 (m, 2H), 7.62–7.59 (m, 1H), 7.57–7.54 (m, 1H), 7.43–7.41 (m, 1H), 3.74–3.71 (m, 2H), 3.66 (t, $J = 4.0$ Hz, 2H), 1.94–1.89 (m, 2H). ^{13}C NMR (100 MHz, $\text{DMSO}-d_6$) δ 169.2, 153.3, 149.9, 143.1, 135.7, 135.2, 134.5, 132.2, 129.2, 127.3, 127.2, 126.1, 125.1, 124.1, 122.9, 59.4, 38.6, 32.2. HRMS (ESI) m/z calcd for $\text{C}_{18}\text{H}_{17}\text{N}_4\text{OS}$ $[\text{M}+\text{H}]^+$ 337.1123, found 337.1106.

4.1.4.12. 3-(Benzo[d]thiazol-2-yl)-2-(N-2-dimethylaminoethyl)aminoquinoxaline (**11e**), 0.154 g, yield 88%, yellow solid, m.p. 77–79 °C, ^1H NMR (400 MHz, $\text{DMSO}-d_6$) δ 9.53 (t, $J = 3.0$ Hz, 1H), 8.19 (d, $J = 5.2$ Hz, 1H), 8.08 (d, $J = 5.4$ Hz, 1H), 7.86 (d, $J = 5.4$ Hz, 1H), 7.67–7.60 (m, 3H), 7.56–7.54 (m, 1H), 7.43–7.40 (m, 1H), 3.69–3.66 (m, 2H), 2.63 (t, $J = 4.0$ Hz, 2H), 2.33 (s, 6H). ^{13}C NMR (100 MHz, $\text{DMSO}-d_6$) δ 169.0, 153.3, 149.8, 143.2, 135.7, 135.3, 134.6, 132.2, 129.2, 127.4, 127.3, 126.1, 125.0, 123.9, 122.9, 57.8, 45.6, 38.9. HRMS (ESI) m/z calcd for $\text{C}_{19}\text{H}_{20}\text{N}_5\text{S}$ $[\text{M}+\text{H}]^+$ 350.1439, found 350.1423.

4.1.4.13. 3-(Benzo[d]thiazol-2-yl)-2-(N-2-morpholino-4-ylethyl)aminoquinoxaline (**11f**), 0.182 g, yield 93%, pale yellow solid, m.p. 151–152 °C, ^1H NMR (400 MHz, $\text{DMSO}-d_6$) δ 9.49 (t, $J = 2.8$ Hz, 1H), 8.23 (d, $J = 5.2$ Hz, 1H), 8.16 (d, $J = 5.4$ Hz, 1H), 7.90 (d, $J = 5.5$ Hz, 1H), 7.70–7.65 (m, 3H), 7.60–7.57 (m, 1H), 7.46–7.43 (m, 1H), 3.78–3.75 (m, 2H), 3.71–3.70 (m, 4H), 2.72 (t, $J = 4.0$ Hz, 2H), 2.55 (s, 4H). ^{13}C NMR (100 MHz, $\text{DMSO}-d_6$) δ 169.2, 153.5, 149.8, 143.2, 135.7, 135.3, 134.6, 132.3, 129.2, 127.5, 127.3, 126.2, 125.2, 123.7, 123.0, 67.0, 56.8, 53.6, 37.8. HRMS (ESI) m/z calcd for $\text{C}_{21}\text{H}_{22}\text{N}_5\text{OS}$ $[\text{M}+\text{H}]^+$ 392.1545, found 392.1526.

4.1.4.14. 3-(Benzo[d]oxazol-2-yl)-2-(N-3-dimethylaminopropyl)aminoquinoxaline (**12a**), 0.159 g, yield 91%, pale yellow solid, m.p. 61–63 °C, ^1H NMR (400 MHz, $\text{DMSO}-d_6$) δ 8.99 (t, $J = 5.4$ Hz, 1H), 7.94–7.91 (m, 3H), 7.69–7.65 (m, 1H), 7.64–7.62 (m, 1H), 7.58–7.54 (m, 1H), 7.52–7.49 (m, 1H), 7.44–7.42 (m, 1H), 3.69–3.65 (m, 2H), 2.41 (t, $J = 6.7$ Hz, 2H), 2.21 (s, 6H), 1.87–1.82 (m, 2H). ^{13}C

NMR (100 MHz, DMSO-*d*₆) δ 160.0, 150.5, 150.1, 143.0, 140.6, 135.9, 132.5, 129.7, 129.5, 127.7, 126.2, 126.0, 125.2, 120.8, 112.0, 57.4, 45.7, 39.4, 26.6. HRMS (ESI) m/z calcd for C₂₀H₂₂N₅O [M+H]⁺ 348.1824, found 348.1809.

4.1.4.15. 3-(Benzo[d]oxazol-2-yl)-2-(N-3-morpholino-4-ylpropyl)aminoquinoxaline (**12b**), 0.182 g, yield 93%, pale yellow solid, m.p. 118–119 °C, ¹H NMR (400 MHz, DMSO-*d*₆) δ 8.91 (t, J = 5.5 Hz, 1H), 7.97–7.93 (m, 3H), 7.71–7.68 (m, 1H), 7.64 (d, J = 8.3 Hz, 1H), 7.59–7.57 (m, 1H), 7.53–7.51 (m, 1H), 7.47–7.44 (m, 1H), 3.72–3.69 (m, 2H), 3.60 (t, J = 4.5 Hz, 4H), 2.45 (t, J = 6.9 Hz, 2H), 2.40 (s, 4H), 1.91–1.86 (m, 2H). ¹³C NMR (100 MHz, DMSO-*d*₆) δ 160.1, 150.6, 150.1, 143.0, 140.6, 132.6, 129.7, 127.7, 126.2, 126.1, 125.3, 120.8, 112.0, 66.7, 56.3, 53.9, 39.1, 25.6. HRMS (ESI) m/z calcd for C₂₂H₂₄N₅O₂ [M+H]⁺ 390.1930, found 390.1912.

4.1.4.16. 3-(Benzo[d]oxazol-2-yl)-2-(N-3-(1H-Imidazol-1-ylpropyl)aminoquinoxaline (**12c**), 0.169 g, yield 90%, pale yellow solid, m.p. 177–178 °C, ¹H NMR (400 MHz, DMSO-*d*₆) δ 8.88 (t, J = 5.5 Hz, 1H), 7.98–7.95 (m, 3H), 7.71–7.69 (m, 2H), 7.65–7.64 (m, 1H), 7.59–7.56 (m, 1H), 7.53–7.51 (m, 1H), 7.47–7.45 (m, 1H), 7.26 (s, 1H), 6.91 (s, 1H), 4.15 (t, J = 6.9 Hz, 2H), 3.65–3.62 (m, 2H), 2.23–2.19 (m, 2H). ¹³C NMR (100 MHz, DMSO-*d*₆) δ 160.1, 150.5, 150.1, 142.8, 140.6, 137.8, 136.0, 132.6, 129.7, 129.6, 128.9, 127.7, 126.3, 126.0, 125.4, 121.0, 119.8, 112.0, 44.4, 38.2, 30.5. HRMS (ESI) calcd for C₂₁H₁₉ON₆ [M+H]⁺ 371.1620, found 371.1603.

4.1.4.17. 3-(3-(Benzo[d]oxazol-2-yl)-2-(N-3-hydroxylpropyl)aminoquinoxaline (**12d**), 0.151 g, yield 94%, yellow solid, m.p. 188–189 °C, ¹H NMR (400 MHz, DMSO-*d*₆) δ 8.90 (t, J = 4.8 Hz, 1H), 7.93–7.91 (m, 3H), 7.67–7.62 (m, 2H), 7.55 (t, J = 7.7 Hz, 1H), 7.49 (t, J = 7.5 Hz, 1H), 7.43–7.41 (m, 1H), 3.71–3.68 (m, 2H), 3.62 (t, J = 6.1 Hz, 2H), 1.92–1.87 (m, 2H). ¹³C NMR (100 MHz, DMSO-*d*₆) δ 160.0, 150.5, 150.1, 142.9, 140.6, 135.8, 132.5, 129.7, 129.5, 127.6, 126.2, 125.9, 125.2, 120.9, 111.9, 59.2, 38.5, 32.3. HRMS (ESI) m/z calcd for C₁₈H₁₇N₄O₂ [M+H]⁺ 321.1351, found 321.1335.

4.1.4.18. 3-(Benzo[d]oxazol-2-yl)-2-(N-2-dimethylaminoethyl)aminoquinoxaline (**12e**), 0.131 g, yield 78%, pale yellow solid, m.p. 86–87 °C, ¹H NMR (400 MHz, DMSO-*d*₆) δ 9.07 (t, J = 4.8 Hz, 1H), 7.95–7.93 (m, 2H), 7.90 (d, J = 7.8 Hz, 1H), 7.69–7.67 (m,

1H), 7.64 (dd, $J = 5.5$, 0.6 Hz, 1H), 7.58–7.55 (m, 1H), 7.52–7.49 (m, 1H), 7.45–7.42 (m, 1H), 3.70–3.67 (m, 2H), 2.62 (t, $J = 6.2$ Hz, 2H), 2.30 (s, 6H). ^{13}C NMR (100 MHz, DMSO- d_6) δ 160.0, 150.5, 150.1, 143.0, 140.6, 135.9, 132.5, 129.7, 129.5, 127.7, 126.2, 126.0, 125.2, 120.9, 112.0, 57.9, 45.7, 39.1. HRMS (ESI) m/z calcd for $\text{C}_{19}\text{H}_{20}\text{N}_5\text{O}$ $[\text{M}+\text{H}]^+$ 334.1668, found 334.1651.

4.1.4.19. 3-(Benzo[d]oxazol-2-yl)-2-(N-2-morpholino-4-ylethyl)aminoquinoxaline (**12f**), 0.155 g, yield 82%, pale yellow solid, m.p. 152–153 °C, ^1H NMR (500 MHz, DMSO- d_6) δ 9.22 (s, 1H), 7.94 (d, $J = 8.1$ Hz, 2H), 7.88 (d, $J = 7.7$ Hz, 1H), 7.70–7.63 (m, 2H), 7.59–7.52 (m, 2H), 7.44 (t, $J = 7.4$ Hz, 1H), 3.70 (d, $J = 3.8$ Hz, 6H), 2.69 (t, $J = 6.0$ Hz, 2H), 2.53 (s, 4H). ^{13}C NMR (125 MHz, DMSO- d_6) δ 160.0, 150.5, 150.1, 143.0, 140.7, 123.5, 129.7, 129.6, 127.7, 126.2, 126.1, 125.2, 120.6, 112.0, 67.0, 56.5, 53.5, 37.9. HRMS (ESI) m/z calcd for $\text{C}_{21}\text{H}_{22}\text{N}_5\text{O}_2$ $[\text{M}+\text{H}]^+$ 376.1773, found 376.1757.

4.1.4.20. 3-(5-Chlorobenzo[d]oxazol-2-yl)-2-(N-3-dimethylaminopropyl)aminoquinoxaline (**15a**), 0.085 g, yield 51 %, pale yellow solid, m.p. 126–127 °C, ^1H NMR (400 MHz, CDCl_3) δ 8.90 (s, 1H), 8.04–8.02 (m, 1H), 7.82–7.81 (m, 1H), 7.72–7.61 (m, 3H), 7.45–7.38 (m, 2H), 3.83–3.87 (m, 2H), 2.51 (t, $J = 7.1$ Hz, 2H), 2.32 (s, 6H), 2.02–1.95 (m, 2H). ^{13}C NMR (100 MHz, CDCl_3) δ 161.2, 150.7, 148.8, 143.6, 141.9, 136.1, 132.2, 130.8, 129.7, 128.7, 127.2, 126.3, 124.8, 120.3, 112.3, 57.6, 45.6, 39.4, 27.1. HRMS (ESI) m/z calcd for $\text{C}_{20}\text{H}_{21}\text{ClN}_5\text{O}$ $[\text{M}+\text{H}]^+$ 382.1429, found 382.1418.

4.1.4.21. 3-(5-Methylbenzo[d]oxazol-2-yl)-2-(N-3-dimethylaminopropyl)aminoquinoxaline (**16a**), 0.043 g, yield 27 %, pale yellow solid, m.p. 122–124 °C, ^1H NMR (400 MHz, CDCl_3) δ 9.08 (s, 1H), 8.05 (d, $J = 8.3$ Hz, 1H), 7.71 (d, $J = 8.3$ Hz, 1H), 7.64–7.60 (m, 3H), 7.42–7.38 (m, 1H), 7.28 (s, 1H), 3.84 (dd, $J = 12.4$, 6.7 Hz, 2H), 2.58 (t, $J = 7.3$ Hz, 2H), 2.52 (s, 3H), 2.36 (s, 6H), 2.05–2.02 (m, 2H). ^{13}C NMR (100 MHz, CDCl_3) δ 160.0, 150.7, 148.6, 143.3, 141.0, 136.1, 135.2, 131.8, 129.7, 129.5, 128.2, 126.2, 124.7, 120.3, 111.0, 57.4, 45.3, 39.2, 26.9, 21.6. HRMS (ESI) m/z calcd for $\text{C}_{21}\text{H}_{24}\text{N}_5\text{O}$ $[\text{M}+\text{H}]^+$ 362.1975, found 362.1968.

4.1.4.22. 3-(5-(Tert-butyl)benzo[d]oxazol-2-yl)-2-(N-3-dimethylaminopropyl)aminoquinoxaline (**17a**), 0.092 g, yield 52 %, pale yellow solid, m.p. 111–112 °C, ^1H NMR

(400 MHz, CDCl₃) δ 9.07 (t, J = 5.2 Hz, 1H), 8.03 (dd, J = 8.3, 1.0 Hz, 1H), 7.82 (d, J = 1.5 Hz, 1H), 7.69–7.67 (m, 1H), 7.65–7.63 (m, 1H), 7.60–7.56 (m, 1H), 7.52 (dd, J = 8.7, 1.9 Hz, 1H), 7.38–7.34 (m, 1H), 3.80 (dd, J = 12.4, 6.9 Hz, 2H), 2.30 (s, 6H), 2.02–1.95 (m, 2H), 1.40 (s, 9H). ¹³C NMR (100 MHz, CDCl₃) δ 159.0, 149.6, 147.8, 147.3, 142.2, 139.7, 135.0, 130.6, 128.6, 128.4, 125.1, 123.7, 123.5, 115.8, 109.7, 56.5, 44.5, 38.2, 34.0, 30.7, 26.1. HRMS (ESI) m/z calcd for C₂₄H₃₀N₅O [M+H]⁺ 404.2445, found 404.2440.

4.1.4.23. 3-(6-Chlorobenzo[d]oxazol-2-yl)-2-(N-3-dimethylaminopropyl)aminoquin-oxaline (**18a**), 0.144 g, yield 86 %, pale yellow solid, m.p. 166–167 °C, ¹H NMR (400 MHz, CDCl₃) δ 8.92 (s, 1H), 8.03 (d, J = 8.3 Hz, 1H), 7.76–7.70 (m, 3H), 7.65–7.61 (m, 3H), 7.43–7.38 (m, 2H), 7.83–7.78 (m, 2H), 2.53–2.50 (m, 2H), 2.30 (s, 6H), 2.03–1.93 (m, 2H). ¹³C NMR (100 MHz, CDCl₃) δ 160.6, 150.7, 150.5, 143.5, 139.6, 136.1, 132.6, 132.1, 129.7, 128.8, 126.3, 126.1, 124.8, 121.0, 112.1, 57.6, 45.6, 39.4, 27.1. HRMS (ESI) m/z calcd for C₂₀H₂₁ClN₅O [M+H]⁺ 382.1429, found 382.1426.

4.1.4.24. 3-(6-Methylbenzo[d]oxazol-2-yl)-2-(N-3-dimethylaminopropyl)aminoquin-oxaline (**19a**), 0.078 g, yield 60 %, pale yellow solid, m.p. 121–123 °C, ¹H NMR (400 MHz, CDCl₃) δ 9.09 (s, 1H), 8.06–8.04 (m, 1H), 7.72–7.70 (m, 2H), 7.64–7.60 (m, 1H), 7.55 (s, 1H), 7.42–7.38 (m, 1H), 7.25 (d, J = 8.6 Hz, 1H), 3.84–3.79 (m, 2H), 2.57–2.53 (m, 5H), 2.34 (s, 6H), 2.06–1.98 (m, 2H). ¹³C NMR (100 MHz, CDCl₃) δ 159.5, 150.7, 150.6, 143.2, 138.7, 137.7, 136.1, 131.7, 129.6, 129.5, 126.6, 126.2, 124.6, 119.8, 111.6, 57.5, 45.5, 39.3, 27.0, 22.1. HRMS (ESI) m/z calcd for C₂₁H₂₄N₅O [M+H]⁺ 362.1975, found 362.1970.

4.1.4.25. 3-(Naphtho[1,2-d]oxazol-2-yl)-2-(N-3-dimethylaminopropyl)aminoquin-oxaline (**20a**), 0.068 g, yield 39 %, pale yellow solid, m.p. 144–145 °C, ¹H NMR (400 MHz, CDCl₃) δ 9.19 (s, 1H), 8.55–8.54 (m, 1H), 8.07–7.98 (m, 2H), 7.89–7.86 (m, 2H), 7.74–7.72 (m, 2H), 7.64–7.59 (m, 2H), 7.43–7.39 (m, 1H), 3.87–3.86 (m, 2H), 2.67 (t, J = 6.9 Hz, 2H), 2.40 (s, 6H), 2.16–2.10 (m, 2H). ¹³C NMR (100 MHz, CDCl₃) δ 159.1, 150.5, 148.1, 143.1, 136.4, 136.2, 131.7, 131.4, 129.6, 129.5, 128.9, 128.2, 127.6, 126.2, 126.0, 124.7, 122.0, 111.4, 57.5, 45.4, 39.2, 27.1. HRMS (ESI) m/z calcd for C₂₄H₂₄N₅O [M+H]⁺ 398.1976, found 398.1974.

4.1.4.26. 3-(5-Chlorobenzo[d]oxazol-2-yl)-2-(N-3-diethylaminopropyl)aminoquin-oxaline (**15g**), 0.033 g, yield 18.5 %, pale yellow solid, m.p. 111–112 °C, ¹H NMR (500 MHz, CDCl₃) δ 8.86 (s, 1H), 8.04 (d, *J* = 8.3 Hz, 1H), 7.81–7.80 (m, 1H), 7.72–7.62 (m, 3H), 7.45–7.39 (m, 2H), 3.80–3.76 (m, 2H), 2.69–2.66 (m, 2H), 2.63 (dd, *J* = 11.4, 5.7 Hz, 4H), 2.01–1.95 (m, 2H), 1.08 (t, *J* = 5.7 Hz, 6H). ¹³C NMR (125 MHz, CDCl₃) δ 161.2, 150.7, 148.8, 143.6, 141.9, 136.1, 132.2, 130.8, 129.7, 128.7, 127.2, 126.3, 124.8, 120.3, 112.3, 50.5, 47.1, 39.5, 26.6, 11.7. HRMS (ESI) *m/z* calcd for C₂₂H₂₅ClN₅O [M+H]⁺ 410.1742, found 410.1735.

4.1.4.27. 3-(5-Methylbenzo[d]oxazol-2-yl)-2-(N-3-diethylaminopropyl)aminoquin-oxaline (**16g**), 0.060 g, yield 35 %, pale yellow solid, m.p. 87–88 °C, ¹H NMR (400 MHz, CDCl₃) δ 9.08 (s, 1H), 8.06 (d, *J* = 8.3 Hz, 1H), 7.71 (d, *J* = 8.4 Hz, 1H), 7.65–7.63 (m, 3H), 7.41 (t, *J* = 9.5 Hz, 1H), 7.29–7.27 (m, 1H), 3.84–3.79 (m, 2H), 2.84–2.80 (m, 2H), 2.76–2.74 (m, 4H), 2.52 (s, 3H), 2.09 (t, *J* = 7.0 Hz, 2H), 1.17 (t, *J* = 7.1 Hz, 6H). ¹³C NMR (100 MHz, CDCl₃) δ 159.9, 150.7, 148.6, 143.2, 141.0, 136.1, 135.3, 131.8, 129.7, 129.5, 128.2, 126.2, 124.8, 120.3, 111.0, 50.2, 46.9, 39.2, 25.8, 21.6, 11.0. HRMS (ESI) *m/z* calcd for C₂₃H₂₈N₅O [M+H]⁺ 390.2288, found 390.2276.

4.1.4.28. 3-(5-(Tert-butyl)benzo[d]oxazol-2-yl)-2-(N-3-diethylaminopropyl)amino-quin-oxaline (**17g**), 0.129 g, yield 68 %, pale yellow oil, ¹H NMR (400 MHz, CDCl₃) δ 9.07 (t, *J* = 5.1 Hz, 1H), 8.04 (dd, *J* = 8.3, 1.0 Hz, 1H), 7.83–7.82 (m, 1H), 7.70 (dd, *J* = 8.4, 0.9 Hz, 1H), 7.64 (d, *J* = 8.7, 1H), 7.61–7.57 (m, 1H), 7.52 (dd, *J* = 8.7, 1.9 Hz, 1H), 7.38–7.34 (m, 1H), 3.78–3.73 (m, 2H), 2.69–2.66 (m, 2H), 2.63 (q, *J* = 7.2 Hz, 4H), 2.01–1.94 (m, 2H), 1.40 (s, 9H), 1.08 (t, *J* = 7.2 Hz, 6H). ¹³C NMR (100 MHz, CDCl₃) δ 160.1, 150.7, 148.8, 148.3, 143.3, 140.8, 136.0, 131.7, 129.6, 129.4, 126.2, 124.8, 124.5, 116.8, 110.7, 50.5, 47.0, 39.5, 35.0, 31.7, 26.6, 11.8. HRMS (ESI) *m/z* calcd for C₂₆H₃₄N₅O [M+H]⁺ 432.2758, found 432.2754.

4.1.4.29. 3-(6-Chlorobenzo[d]oxazol-2-yl)-2-(N-3-diethylaminopropyl)aminoquin-oxaline (**18g**), 0.118 g, yield 69 %, pale yellow solid, m.p. 77–78 °C, ¹H NMR (400 MHz, CDCl₃) δ 8.88 (s, 1H), 8.03 (t, *J* = 8.4 Hz, 1H), 7.76–7.71 (m, 3H), 7.67–7.62 (m, 1H), 7.44–7.39 (m, 2H), 3.81–3.76 (m, 2H), 2.68 (t, *J* = 7.2 Hz, 2H), 2.65–2.59

(m, 4H), 2.02–1.95 (m, 2H), 1.12–1.07 (m, 6H). ^{13}C NMR (100 MHz, CDCl_3) δ 160.6, 150.7, 150.5, 143.5, 139.6, 136.1, 132.6, 132.1, 129.7, 128.8, 126.3, 126.1, 124.8, 120.9, 112.1, 50.5, 47.1, 39.5, 26.6, 11.7. HRMS (ESI) m/z calcd for $\text{C}_{22}\text{H}_{25}\text{ClN}_5\text{O}$ $[\text{M}+\text{H}]^+$ 410.1724, found 410.1736.

4.1.4.30. 3-(6-Methylbenzo[d]oxazol-2-yl)-2-(N-3-diethylaminopropyl)aminoquin-oxaline (**19g**), 0.120 g, yield 70 %, pale yellow oil, ^1H NMR (400 MHz, CDCl_3) δ 9.01 (t, $J = 5.1$ Hz, 1H), 8.03 (dd, $J = 8.3, 1.0$ Hz, 1H), 7.70 (dd, $J = 8.4, 1.0$ Hz, 1H), 7.65–7.63 (m, 1H), 7.61–7.56 (m, 1H), 7.50 (s, 1H), 7.38–7.34 (m, 1H), 7.20 (dd, $J = 8.2, 0.8$ Hz, 1H), 3.77–3.72 (m, 2H), 2.68–2.64 (m, 2H), 2.62 (q, $J = 7.2$ Hz, 4H), 2.50 (s, 3H), 2.00–1.93 (m, 2H), 1.06 (t, $J = 7.1$ Hz, 6H). ^{13}C NMR (100 MHz, CDCl_3) δ 159.5, 150.6, 150.5, 143.2, 138.6, 137.6, 136.0, 131.6, 129.6, 129.4, 126.6, 126.2, 124.5, 119.8, 111.5, 50.5, 47.0, 39.5, 26.5, 22.0, 11.7. HRMS (ESI) m/z calcd for $\text{C}_{23}\text{H}_{28}\text{N}_5\text{O}$ $[\text{M}+\text{H}]^+$ 390.2288, found 390.2286.

4.1.4.31. 3-(Naphtho[1,2-d]oxazol-2-yl)-2-(N-3-diethylaminopropyl)aminoquinoxaline (**20g**), 0.094 g, yield 50 %, pale yellow solid, m.p. 121–122 °C, ^1H NMR (400 MHz, CDCl_3) δ 9.15 (s, 1H), 8.55–8.53 (m, 1H), 8.06 (d, $J = 8.3$ Hz, 1H), 8.01–8.00 (m, 1H), 7.92–7.87 (m, 2H), 7.74–7.70 (m, 2H), 7.65–7.60 (m, 2H), 7.43–7.39 (m, 1H), 3.84 (d, $J = 5.8$ Hz, 2H), 2.77 (t, $J = 7.2$ Hz, 2H), 2.69 (q, $J = 7.2$ Hz, 4H), 2.15–2.05 (m, 2H), 1.10 (t, $J = 7.2$ Hz, 6H). ^{13}C NMR (100 MHz, CDCl_3) δ 159.2, 150.5, 148.1, 143.2, 136.4, 136.1, 131.6, 131.4, 129.6, 129.5, 128.9, 128.2, 127.5, 126.2, 126.0, 124.7, 122.0, 111.4, 50.8, 47.1, 39.6, 26.9, 11.7. HRMS (ESI) m/z calcd for $\text{C}_{26}\text{H}_{28}\text{N}_5\text{O}$ $[\text{M}+\text{H}]^+$ 426.2289, found 426.2283.

4.2. Biological activity

4.2.1. Anti-proliferative activity

Cells were seeded in 96-well plates and incubated overnight in 180 μL of medium containing 10% Fetal Bovine Serum (Gibco, USA). On the following day, 20 μL of compounds at different concentrations were added to each well and incubated for 48 h. Then, 10 μL of 5 mg/mL MTT solution was added into each well and incubated for 4 h at 37 °C. The culture medium was then removed, and 100 μL of

DMSO was added to dissolve the formazan dye before measuring the absorbance at 570 nm in a multiwell plate reader. Cell viability was calculated using the following formula: cell viability (%) = $(A_{570e}/A_{570c}) \times 100\%$, A_{570e} and A_{570c} represented the absorbance values from the experimental and control groups, respectively.

4.2.2. DNA intercalation assay

250 ng of negatively supercoiled pBR322 DNA was incubated with EB, the selected compounds at concentrations of 50 μM , or the indicated concentrations of **12a** in a total volume of 10 μL at 37 °C for 1h. Then, the reaction was terminated by the addition of 2 mL loading buffer (0.25% bromophenol blue, xylene cyanol EF 0.25% and 40% glycerol). The samples were electrophoresed on a 1.5% agarose gel and stained with 0.5 $\mu\text{g}\cdot\text{mL}^{-1}$ EB. DNA bands were visualized by transillumination with UV light.

4.2.3. DNA Topo I inhibitory assay

A mixture of 1 U of Topoisomerase I, the indicated concentrations of CPT, the tested compounds at concentrations of 50 μM , or the indicated concentrations of **12a** was incubated at 37 °C in Topo I buffer for 30 min. Then, 250 ng of pBR322 DNA was added in a total volume of 10 μL and further incubated at 37 °C for 30 min. The reaction was terminated by the addition of 2 mL loading buffer, and the mixture was electrophoresed on a 1% agarose gel in 1 \times TAE buffer for 90 min at 80 V and stained 0.5 $\mu\text{g}/\text{mL}$ of EB. DNA bands were visualized by transillumination with UV light.

4.2.4. Topo I-mediated DNA-unwinding assay

A mixture of 5 U of Topoisomerase I, 250 ng pBR322 DNA was incubated at 37 °C in Topo I buffer for 30 min. Then, the indicated concentrations of CPT or EB, 50 μM the tested compounds, or the indicated concentrations of **12a** was added in a total volume of 10 μL and further incubated at 37 °C for 30 min. The reaction was terminated by the addition of 2 mL loading buffer. The mixture was electrophoresed on a 1% agarose gel in 1 \times TAE buffer for 90 min at 80 V and stained with 0.5 $\mu\text{g}/\text{mL}$ of EB. DNA bands were visualized by transillumination with UV light.

4.2.5. Cell apoptosis assay

MGC-803 cells were seeded at a concentration of 2×10^6 cells/mL in DMEM medium with 10% FBS in 6-well plates with a final media volume of 2 mL. The plates were incubated overnight after treatment with different concentrations compound **12a** for 24 h. Cells were collected and washed with cold PBS three times, resuspended in $1 \times$ Binding Buffer at a density of 1×10^6 cells/mL, stained with FITC Annexin V and PI for 20 min at 25 °C in the dark, and analyzed on a flow cytometer equipped with a 488 nm argon laser (Becton-Dickinson). Analysis was performed using the system software (Cell Quest).

4.2.6. Cell cycle assay

The MGC-803 cells line was treated with different concentrations of compound **12a** and incubated for 48 h, followed centrifugation at 1200 rpm for 6 min. Cells were washed twice with PBS and then fixed with ice-cold 70% ethanol in PBS at -20 °C overnight. The cells were treated with 100 µg/mL of RNase A in the dark at 37 °C in a water bath for 30 min before washing with PBS, and staining with 1 mg/mL propidium iodide (PI) in the dark at 37 °C for 5 min. Analysis was performed with the ModFit LT software.

4.2.7. ROS generation assay

MGC-803 cells were seeded into six-well plates, cultured to 80% confluency, and treated with compound **12a** at concentrations of 2.5, 5 and 10 µM for 24 h. The cells were harvested, washed with ice-cold PBS, and incubated with DCFH-DA (in a final concentration of 100 µM) at 37 °C for 20 min in the dark. Finally, the cells were resuspended in 500 µL of PBS and analyzed on a flow cytometer equipped with a 488 nm argon laser (Becton-Dickinson)

4.2.8. Intracellular Ca^{2+} assay

MGC-803 cells were seeded into six-well plates at a concentration of 2×10^6

cells/mL in DMEM medium with 10% FBS and treated with compound **12a** at concentrations of 2.5, 5 and 10 μ M for 24 h. The cells were harvested, washed once with ice-cold PBS, and incubated with Fluo-3 AM (5 μ M in a final concentration) at 37 °C for 20 min in the dark. Finally, the cells were resuspended in 500 μ L of PBS and analyzed on a flow cytometer equipped with a 525 nm excitation wavelength laser (Becton- Dickinson)

4.2.9. Mitochondrial membrane potential assay

MGC-803 cells (1×10^6 cells) were seeded in six-well tissue culture plates and **12a** was added to the culture medium (2.5, 5.0, 10 μ M in a final concentration). After incubation for 24 h at 37 °C, the cells were harvested, washed once with ice-cold PBS, and incubated with 5 μ g/mL fluorescent probe JC-1 at 37 °C for 20 min in the dark. Finally, the cells were resuspended in 500 μ L of PBS and analyzed on a flow cytometer equipped with a 488 nm excitation wavelength laser (Becton- Dickinson).

4.2.10. Western Blotting assay

MGC-803 cells were grown in 100 mm tissue culture dishes at 1×10^6 cells until 80% confluency. The cells were treated with **12a** at indicated concentrations for 24 h, washed once with ice-cold PBS followed by a lysis buffer solution (50 mM Tris HCl, 300 mM NaCl, 1% Triton X-100, 10% glycerol, 1.5 mM $MgCl_2$, 1 mM $CaCl_2$, 1 mM PMSF and 1% protease inhibitor cocktail). 50 μ g of protein was loaded onto a 10 or 12% SDS-PAGE, electrophoresed, and transferred to a PVDF membrane (Millipore, USA). The membranes were blocked with 5% skim milk in Tris buffered saline containing 0.1% tween 20 (TBST) and probed with primary antibodies at a dilution of 1:1000 at 4 °C overnight. The blots were washed, exposed to HRP-conjugated anti-rabbit IgG (Cell Signaling Technology Inc, USA) at a dilution of 1:2000 at 25 °C for 2 h, and visualized by an ECL Western blot system (Kodak, USA).

4.2.11. In vitro assay of caspase-3/9 activity

The assay was performed based on the ability of the active enzyme to cleave the chromophore from the enzyme substrate FITC-DEVD-FMK (for caspase-3) or FITC-

LEHD-FMK (for caspase-9). The **12a**-treated cells and control cells were harvested at a density of 1×10^6 cells/mL in RPMI 1640 medium supplemented with 10% FCS. 300 μ L each of the induced and control cultures were incubated with 1 μ L of FITCDEVD-FMK or FITC-LEHD-FMK for 1 h in a 37 °C incubator with 5% CO₂. Flow cytometric analysis was performed using a FACS AriaII flow cytometer equipped with a 488 nm argon laser. Results are represented as the percent change of the activity compared to the untreated control.

4.2.12. Molecular docking

Discovery Studio (version 2017R2, BIOVIA, USA) was employed to carry on molecular docking. The crystal structures of the ternary complex (PDB code 1T8I), containing Topo I, DNA, and CPT, was downloaded from the Protein Data Bank (<http://www.rcsb.org>). All bound water and ligands were eliminated from the protein and the polar hydrogen was added. The structures of the ternary complex were prepared and CHARMM force field was employed and the whole Topo I complex was defined as a receptor. The 3D structures of **12a** were generated and minimized and docking into the three-dimensional structure of Topo I following CDOCKER protocol. Types of interactions of the docked protein with ligand were analyzed at the end of molecular docking [50].

4.2.13. In vivo xenograft model assay

The assays were carried out as described previously with minor modifications [33]. Pathogen-free male BALB/C nude mice aged 6 weeks (Changzhou Cavens Experimental Animal Co., Ltd., Changzhou, China) were used to establish the MGC-803 xenograft model. The mice were raised under controlled environmental conditions (12 h light-dark cycle at 24 °C and 60–85% humidity). Solid tumors were introduced by subcutaneous injection of 5×10^6 MGC-803 cells into the flank region of the nude mice ($n = 6$). The tumor-bearing mice were treated i.p. with vehicle (5% DMSO in saline, v/v) or with 6 or 12 $\text{mg} \cdot \text{kg}^{-1}$ **12a** (dissolved in saline to form a solution of 0.6 mg/mL or 1.2 mg/mL, respectively) per 2 days. CPT (6 mg kg^{-1} , per 2 days) was used as a positive control (7.2 mg CPT was dissolved in 0.72 mL DMSO and diluted with 11.28 mL saline to form a solution of 0.6 mg/mL). The tumor size

and body weight of the mice were measured three times a week. The tumor size was determined by measuring the length (l) and width (w) and calculating the volume ($V = lw^2/2$). All data are shown as mean \pm standard deviation (SD) using two-tailed Student t tests and one-way ANOVA with Bonferroni multiple comparison post-test. P less than 0.05 was considered as the threshold for significance.

4.2.14. Statistical analysis

Data are reported as means \pm SD. Statistical analysis was performed using SPSS 17.0 software (Chicago, IL, USA), $P < 0.05$ were considered as statistically significant.

Acknowledgements

This work was supported by the National Natural Science Foundation of China (21462008), the Natural Science Foundation of Guangxi Province (2015GXNSFDA139009, 2017GXNSFDA198045), the Foundation of State Key Laboratory for Chemistry and Molecular Engineering of Medicinal Resources (Guangxi Normal University, CMEMR2018-A1), Ministry of Education of China (IRT_16R15) and Guangxi Medical Talent Highland (201705).

Appendix A. Supplementary data

Supplementary data related to this article can be found at

<https://doi.org/>

References

- [1] W. Chen, J. He, R. Zheng, S. Zhang, H. Zeng, C. Xia, T. Zuo, Z. Yang, X. Zou, Cancer incidence and mortality in China, 2013, *Cancer Lett.* 401 (2017) 63–71.
- [2] W. Chen, R. Zheng, P.D. Baade, S. Zhang, H. Zeng, F. Bray, A. Jemal, X.Q. Yu, J. He, Cancer statistics in China, 2015, *CA Cancer J. Clin.* 66 (2016) 115–132.
- [3] B. Kumar, S. Singh, I. Skvortsova, V. Kumar, Promising Targets in Anti-cancer Drug Development: Recent Updates, *Curr. Med. Chem.* 24 (2017) 4729–4752.
- [4] S.M.V. de Almeida, A.G. Ribeiro, G.C. de Lima Silva, J.E. Ferreira Alves, E.I.C. Beltrao, J.F. de Oliveira, L.B.J. de Carvalho, M.D.C. Alves de Lima, DNA binding and Topoisomerase inhibition: How can these mechanisms be explored to design more specific anticancer agents? *Biomed. Pharmacother.* 96 (2017) 1538–1556.

- [5] G. Capranico, J. Marinello, G. Chillemi, Type I DNA Topoisomerases, *J. Med. Chem.* 60 (2017) 2169–2192.
- [6] Y. Pommier, Drugging Topoisomerases: Lessons and Challenges, *ACS Chem. Biol.* 8 (2013) 82–95.
- [7] C. Sheng, Z. Miao, W. Zhang, New strategies in the discovery of novel non-camptothecin topoisomerase I inhibitors, *Curr. Med. Chem.* 18 (2011) 4389–4409.
- [8] M.K. Kathiravan, A.N. Kale, S. Nilewar, Discovery and Development of Topoisomerase Inhibitors as Anticancer Agents, *Mini-Rev. Med. Chem.* 16 (2016) 1219–1229.
- [9] Y. Pommier, M. Cushman, The indenoisoquinoline noncamptothecin topoisomerase I inhibitors: update and perspectives. *Mol. Cancer Ther.* 8 (2009) 1008–1014.
- [10] Q.-D. You, Z.-Y. Li, C.-H. Huang, Q. Yang, X.-J. Wang, Q.-L. Guo, X.-G. Chen, X.-G. He, T.-K. Li, J.-W. Chern, Discovery of a Novel Series of Quinolone and Naphthyridine Derivatives as Potential Topoisomerase I Inhibitors by Scaffold Modification. *J. Med. Chem.* 52 (2009) 5649–5661.
- [11] P. Diana, A. Martorana, P. Barraja, A. Montalbano, G. Dattolo, G. Cirrincione, F. Dall'Acqua, A. Salvador, D. Vedaldi, G. Basso, G. Viola, Isoindolo[2,1-a]quinoxaline Derivatives, Novel Potent Antitumor Agents with Dual Inhibition of Tubulin Polymerization and Topoisomerase I. *J. Med. Chem.* 51 (2008) 2387–2399.
- [12] J. Kim, H. Kim, S.B. Park, Privileged Structures: Efficient Chemical "Navigators" toward Unexplored Biologically Relevant Chemical Spaces, *J. Am. Chem. Soc.* 136 (2014) 14629–14638.
- [13] J. Polanski, A. Kurczyk, A. Bak, R. Musiol, Privileged structures – dream or reality: preferential organization of azanaphthalene scaffold, *Curr. Med. Chem.* 19 (2012) 1921–1945.
- [14] J.A. Pereira, A.M. Pessoa, M.N.D.S. Cordeiro, R. Fernandes, C. Prudencio, J.P. Noronha, M. Vieira, Quinoxaline, its derivatives and applications: A State of the Art review, *Eur. J. Med. Chem.* 97 (2015) 664–672.
- [15] A.C. Pinheiro, T.C. Mendonca Nogueira, M.V.N. de Souza, Quinoxaline Nucleus: A Promising Scaffold in Anti-cancer Drug Discovery, *Anti-Cancer Agents Med. Chem.* 16 (2016) 1339–1352.
- [16] S.K. Subran, P. Paira, Synthesis and Pharmacological Applications of Certain Quinoxaline Analogues: A Review, *Curr. Bioact. Compd.* 13 (2017) 186–212.
- [17] S. Tariq, K. Somakala, M. Amir, Quinoxaline: An insight into the recent pharmacological advances, *Eur. J. Med. Chem.* 143 (2018) 542–557.
- [18] X. Chen, X. Huan, Y. Chen, J. Ding, Q. Liu, Y. Wang, Q. He, C. Tan, Y. Xu, Z.

- Miao, C. Yang, Design and synthesis of 2-(4,5,6,7-tetrahydrothieno-pyridin-2-yl)-benzoimidazole carboxamides as novel orally efficacious Poly(ADP-ribose)-polymerase (PARP) inhibitors, *Eur. J. Med. Chem.* 145 (2018) 389–403.
- [19] J. Zhou, M. Ji, Z. Zhu, R. Cao, X. Chen, B. Xu, Discovery of 2-substituted 1H-benzo[d]imidazole-4-carboxamide derivatives as novel poly(ADP-ribose)-polymerase-1 inhibitors with in vivo anti-tumor activity, *Eur. J. Med. Chem.* 132 (2017) 26–41.
- [20] J. Zhou, J. Jin, Y. Zhang, Y. Yin, X. Chen, B. Xu, Synthesis and antiproliferative evaluation of novel benzoimidazole-contained oxazole-bridged analogs of combretastatin A-4, *Eur. J. Med. Chem.* 68 (2013) 222–232.
- [21] M. Cindric, S. Jambon, A. Harej, S. Depauw, M.-H. David-Cordonnier, S. Kraljevic Pavelic, G. Karminski-Zamola, M. Hranjec, Novel amidino substituted benzimidazole and benzothiazole benzo[b]thieno-2-carboxamides exert strong antiproliferative and DNA binding properties, *Eur. J. Med. Chem.* 136 (2017) 468–479.
- [22] M.T. Gabr, N.S. El-Gohary, E.R. El-Bendary, M.M. El-Kerdawy, Synthesis and in vitro antitumor activity of new series of benzothiazole and pyrimido[2,1-b]benzothiazole derivatives, *Eur. J. Med. Chem.* 85 (2014) 576–592.
- [23] M. Gjorgjieva, T. Tomasic, M. Barancokova, S. Katsamakas, J. Ilas, P. Tammela, L. Peterlin Masic, D. Kikelj, Discovery of Benzothiazole Scaffold-Based DNA Gyrase B Inhibitors, *J. Med. Chem.* 59 (2016) 8941–8954.
- [24] R.S. Keri, M.R. Patil, S.A. Patil, S. Budagupi, A comprehensive review in current developments of benzothiazole-based molecules in medicinal chemistry, *Eur. J. Med. Chem.* 89 (2015) 207–251.
- [25] J. Ma, G. Bao, L. Wang, W. Li, B. Xu, B. Du, J. Lv, X. Zhai, P. Gong, Design, synthesis, biological evaluation and preliminary mechanism study of novel benzothiazole derivatives bearing indole-based moiety as potent antitumor agents, *Eur. J. Med. Chem.* 96 (2015) 173–186.
- [26] U. Rothweiler, W. Stensen, B.O. Brandsdal, J. Isaksson, F.A. Leeson, R.A. Engh, J.S.M. Svendsen, Probing the ATP-Binding Pocket of Protein Kinase DYRK1A with Benzothiazole Fragment Molecules, *J. Med. Chem.* 59 (2016) 9814–9824.
- [28] A. Rouf, C. Tanyeli, Bioactive thiazole and benzothiazole derivatives, *Eur. J. Med. Chem.* 97 (2015) 911–927.
- [29] C.S. Demmer, L. Bunch, Benzoxazoles and oxazolopyridines in medicinal

- chemistry studies, *Eur. J. Med. Chem.* 97 (2015) 778–785.
- [30] S.K. Gorla, M. Kavitha, M. Zhang, J.E.W. Chin, X. Liu, B. Striepen, M. Makowska-Grzyska, Y. Kim, A. Joachimiak, L. Hedstrom, G.D. Cuny, Optimization of Benzoxazole-Based Inhibitors of *Cryptosporidium parvum* Inosine 5'-Monophosphate Dehydrogenase, *J. Med. Chem.* 56 (2013) 4028–4043.
- [31] P. Malapati, V.S. Krishna, R. Nallangi, R.R. Srilakshmi, D. Sriram, Identification and development of benzoxazole derivatives as novel bacterial glutamate racemase inhibitors, *Eur. J. Med. Chem.* 145 (2018) 23–34.
- [32] W. Zhang, J. Liu, J.M. Macho, X. Jiang, D. Xie, F. Jiang, W. Liu, L. Fu, Design, synthesis and antimicrobial evaluation of novel benzoxazole derivatives, *Eur. J. Med. Chem.* 126 (2017) 7–14.
- [33] G.-H. Zhang, J.-M. Yuan, G. Qian, C.-X. Gu, K. Wei, D.-L. Mo, J.-K. Qin, Y. Peng, Z.-P. Zhou, C.-X. Pan, G.-F. Su, Phthalazino[1,2-b]quinazolinones as p53 Activators: Cell Cycle Arrest, Apoptotic Response and Bak-Bcl-xl Complex Reorganization in Bladder Cancer Cells, *J. Med. Chem.* 60 (2017) 6853–6866.
- [34] A.F.M.M. Rahman, S.-E. Park, A.A. Kadi, Y. Kwon, Fluorescein Hydrazones as Novel Nonintercalative Topoisomerase Catalytic Inhibitors with Low DNA Toxicity, *J. Med. Chem.* 57 (2014) 9139–9151.
- [35] C.-K. Peng, T. Zeng, X.-J. Xu, Y.-Q. Chang, W. Hou, K. Lu, H. Lin, P.-H. Sun, J. Lin, W.-M. Chen, Novel 4-(4-substituted amidobenzyl)furan-2(5H)-one derivatives as topoisomerase I inhibitors, *Eur. J. Med. Chem.* 127 (2017) 187–199.
- [36] B.-L. Yao, Y.-W. Mai, S.-B. Chen, H.-T. Xie, P.-F. Yao, T.-M. Ou, J.-H. Tan, H.-G. Wang, D. Li, S.-L. Huang, L.-Q. Gu, Z.-S. Huang, Design, synthesis and biological evaluation of novel 7-alkylamino substituted benzo[a]phenazin derivatives as dual topoisomerase I/II inhibitors, *Eur. J. Med. Chem.* 92 (2015) 540–553.
- [37] L.-M. Yu, X.-R. Zhang, X.-B. Li, Y. Yang, H.-Y. Wei, X.-X. He, L.-Q. Gu, Z.-S. Huang, Y. Pommier, L.-K. An, Synthesis and biological evaluation of 6-substituted indolizinoquinolinediones as catalytic DNA topoisomerase I inhibitors, *Eur. J. Med. Chem.* 101 (2015) 525–533.
- [38] Y. Pommier, J.M. Covey, D. Kerigan, J. Markovits, R. Pham, DNA unwinding and inhibition of mouse leukemia L1210 DNA topoisomerase I by intercalators, *Nucleic Acids Res.* 15 (1987) 6713–6731.
- [39] B.L. Staker, M.D. Feese, M. Cushman, Y. Pommier, D. Zembower, L. Stewart,

- A.B. Burgin, Structures of Three Classes of Anticancer Agents Bound to the Human Topoisomerase I-DNA Covalent Complex. *J. Med. Chem.* 48 (2005) 2336-2345.
- [40] W. Hou, Z.-Y. Wang, C.-K. Peng, J. Lin, X. Liu, Y.-Q. Chang, J. Xu, R.-W. Jiang, H. Lin, P.-H. Sun, W.-M. Chen, Novel securinine derivatives as topoisomerase I based antitumor agents. *Eur. J. Med. Chem.* 122 (2016) 149-163.
- [41] H.-B. Li, R.-X. Wang, H.-B. Jiang, E.-D. Zhang, J.-Q. Tan, H.-Z. Xu, R.-R. Zhou, X.-B. Xia, Mitochondrial ribosomal protein L10 associates with cyclin B1/Cdk1 activity and mitochondrial function, *DNA Cell Biol.* 35 (2016) 680-690.
- [42] Y. Yang, S. Karakhanova, W. Hartwig, J.G. D'Haese, P.P. Philippov, J. Werner, A.V. Bazhin, Mitochondria and Mitochondrial ROS in Cancer: Novel Targets for Anticancer Therapy, *J. Cell. Physiol.* 231 (2016) 2570-2581.
- [43] R.R.M.L. La, G. Roest, G. Bultynck, J.B. Parys, Intracellular Ca^{2+} signaling and Ca^{2+} microdomains in the control of cell survival, apoptosis and autophagy, *Cell Calcium* 60 (2016) 74-87.
- [44] X. Yun, W. Rao, C. Xiao, Q. Huang, Apoptosis of leukemia K562 and Molt-4 cells induced by emamectin benzoate involving mitochondrial membrane potential loss and intracellular Ca^{2+} modulation, *Environ. Toxicol. Pharmacol.* 52 (2017) 280-287.
- [45] G. Kroemer, L. Galluzzi, C. Brenner, Mitochondrial membrane permeabilization in cell death, *Physiol. Rev.* 87 (2007) 99-163.
- [46] W.A. Siddiqui, A. Ahad, H. Ahsan, The mystery of Bcl-2 family: Bcl-2 proteins and apoptosis: an update, *Arch. Toxicol.* 89 (2015) 289-317.
- [47] Y. Wu, L. Tang, Bcl-2 Family Proteins Regulate Apoptosis and Epithelial to Mesenchymal Transition by Calcium Signals, *Curr. Pharm. Des.* 22 (2016) 4700-4704.
- [48] A. Inoue, K. Takitani, M. Koh, C. Kawakami, T. Kuno, H. Tamai, Induction of Apoptosis by γ -Tocotrienol in Human Cancer Cell Lines and Leukemic Blasts From Patients: Dependency on Bid, Cytochrome c, and Caspase Pathway, *Nutr. Cancer* 63 (2011) 763-770.
- [49] G. Jia, Q. Wang, R. Wang, D. Deng, L. Xue, N. Shao, Y. Zhang, X. Xia, F. Zhi, Y. Yang, Tubeimoside-1 induces glioma apoptosis through regulation of Bax/Bcl-2 and the ROS/Cytochrome C/Caspase-3 pathway, *Onco. Targets Ther.* 8 (2015) 303-311.

- [50] K. Chen, Y.-L. Zhang, J. Fan, X. Ma, Y.-J. Qin, H.-L. Zhu, Novel nicotinoyl pyrazoline derivatives bearing N-methyl indole moiety as antitumor agents: Design, synthesis and evaluation. *Eur. J. Med. Chem.* 156 (2018) 722-737.

Highlights

1. 30 novel 3-benzoylquinoxaline derivatives were rationally designed and synthesized.
2. **12a** exhibits potent antitumor efficacy *in vitro* and *in vivo* with low toxicity.
3. **12a** inhibits the Topo I *via* Topo I-mediated DNA unwinding.
4. **12a** regulates multiple signaling pathways and induces apoptosis in tumor cell.